J. Fluid Mech. (1996), vol. 321, pp. 235–278

Multi-scalar triadic interactions in differential diffusion with and without mean scalar gradients

By P. K. YEUNG

School of Aerospace Engineering, Georgia Institute of Technology, Atlanta, GA 30332, USA
e-mail: yeung@peach.ae.gatech.edu

(Received 23 October 1995 and in revised form 1 April 1996)

The spectral mechanisms of the differential diffusion of pairs of passive scalars with different molecular diffusivities are studied in stationary isotropic turbulence, using direct numerical simulation data at Taylor-scale Reynolds number up to 160 on 128^3 and 256^3 grids. Of greatest interest are the roles of nonlinear triadic interactions between different scale ranges of the velocity and scalar fields in the evolution of spectral coherency between the scalars, and the effects of mean scalar gradients.

Analysis of single-scalar spectral transfer (extending the results of a previous study) indicates a robust local forward cascade behaviour at high wavenumbers, which is strengthened by both high diffusivity and mean gradients. This cascade is driven primarily by moderately non-local interactions in which two small-scale scalar modes are coupled via a lower-wavenumber velocity mode near the peak of the energy dissipation spectrum. This forward cascade is coherent, tending to increase the coherency between different scalars at high wavenumbers but to decrease it at lower wavenumbers. However, at early times coherency evolution at high wavenumbers is dominated by de-correlating effects due to a different type of non-local triad consisting of two scalar modes with a moderate scale separation and a relatively high-wavenumber velocity mode. Consequently, although the small-scale motions play little role in spectral transfer, they are responsible for the rapid de-correlation observed at early times. At later times both types of competing triadic interactions become important over a wider wavenumber range, with increased relative strength of the coherent cascade, so that the coherency becomes slow-changing. When uniform mean scalar gradients are present, a stationary state develops in the coherency spectrum as a result of a balance between a coherent mean gradient contribution (felt within about 1 eddy-turnover time) and the net contribution from scale interactions. The latter is made less de-correlating because of a strengthened coherent forward cascade, which is in turn caused by uniform mean gradients acting as a primarily low-wavenumber source of scalar fluctuations with the same spectral content as the velocity field.

1. Introduction

Efficient mixing is one of the most important characteristics of turbulent flows. As pointed out early by Corrsin (1951) and Batchelor (1959), a net effect of advection by the turbulent velocity fluctuations is to break concentrated blobs of scalar into smaller, more disorganized, fragments. As scalar fluctuations are generated by this process at progressively smaller scales, ultimately localized inhomogeneities at the small scales accompanied by large spatial gradients are rapidly smeared out by molecular diffusion.

Since both velocity and scalar fluctuations span a range of scales (which widens with increasing Reynolds and Péclet numbers), turbulent scalar transport is closely related to complex couplings between different scales in the hydrodynamic and scalar fields.

The nature of nonlinear interactions between different scale sizes is a central issue in turbulence research, underlying such pivotal concepts as the Kolmogorov (1941) similarity hypotheses and local isotropy for turbulence at high Reynolds number. In homogeneous turbulence these interactions are conveniently studied using a Fourier-spectral approach, in which turbulent fluctuations are decomposed into contributions from different scale sizes via a transformation to Fourier (wavenumber) space. The role of triadic interactions in energy transfer has recently received considerable attention (Domaradzki & Rogallo 1990; Brasseur & Wei 1994; Zhou 1993*a*,*b* and others), and the implications of the possibility of departures of the small scales from local isotropy have been explored by numerical experiments (Yeung & Brasseur 1991; Yeung, Brasseur & Wang 1995).

Extensions of the Kolmogorov hypotheses to the prediction of spectral forms of scalar fields (Obukhov 1949 and Corrsin 1951) are well-known, although they are less well supported by experiment (Sreenivasan 1991). In contrast to the status of energy transfer, the detailed mechanisms of spectral transfer in scalars have been studied very little, except for some one-dimensional measurements by Yeh & Van Atta (1973). In Fourier space, the nonlinear convective term in the scalar transport equation is given by a convolution integral which represents the cumulative effect of triadic interactions, where each triad is a closed triangle in wavenumber space consisting of two scalar modes coupled via a velocity mode. Using direct numerical simulation (DNS) data and an extension of a technique of Domaradzki & Rogallo (1990), Yeung (1994) studied the roles of different geometric classes of triadic interactions in the spectral transfer of a single passive scalar at Taylor-scale Reynolds number (R_λ) equal to 38. The main conclusion in Yeung (1994) was that at high wavenumbers the dominant process is a local forward cascade in the scalar field driven primarily by non-local interactions that couple two scalar modes at similarly high wavenumber via a low-wavenumber velocity mode. This spectral space representation is consistent with the physical space arguments given by Corrsin (1951) and Batchelor (1959).

In many practical applications of turbulent mixing, such as simultaneous heat and mass transfer in industrial processes and the inter-diffusion of multiple chemical species in turbulent flames, more than one scalar is involved. For two-scalar mixing, two important simplifications apply in the case of equal diffusivities: (*a*) if the scalars are non-reacting and passive then each scalar satisfies the same evolution equation and linear superposition can be employed, and (*b*) even if the scalars are reacting a linear combination of the species concentrations can be found such that they are conserved (which constitutes the Shvab–Zeldovich conserved-scalar approach in combustion literature). Komori *et al.* (1991) used a stochastic model to calculate the correlation between initially segregated reacting species of equal diffusivities. However, the case of multi-scalar mixing with different molecular diffusivities is considerably more complex and less understood. The importance of accurately accounting for the differential diffusion with different diffusivities in combustion models is now well recognized (Bilger & Dibble 1982; Pope 1990).

Several recent efforts at understanding differential diffusion have been directed at the simpler case of passive scalars, with emphasis on evolution from identical initial conditions. Direct numerical simulations of differential diffusion for decaying scalar fields have been conducted in both stationary (Yeung & Pope 1993) and decaying (Nilsen & Kosály 1996) isotropic turbulence. Saylor & Sreenivasan (1993)

performed inert colour dye experiments at high Schmidt number in water jets, and found significant effects of differential diffusion even at scales much larger than the Batchelor scale. Kerstein, Cremer & McMurtry (1995) also used stochastic simulations and a linear-eddy mixing model to investigate the scaling properties of differential diffusion, and suggested that the mean-square difference between two scalars decreases inversely as the square root of the Reynolds number. In addition, Smith (1994) performed experiments in both reacting and non-reacting turbulent jets, which suggested that high-order statistics sensitive to the small scales may continue to be affected by differential diffusion at high Reynolds numbers.

An important tool used to describe the scale dependency of the correlation between multiple scalars is the coherency spectrum, also known as (spectral) coherence. Measurements of the coherency spectrum in the frequency domain have been reported by Li, Brown & Bilger (1993) for a reactive-scalar mixing layer. The experimental results, which agree well with a theory given by Kosály (1993), indicate that near the centreline the scalars are highly correlated at low frequency, but nearly uncorrelated at high frequency. Measurements have also been made for a pair of heat sources of the same diffusivity, invoking the principle of superposition (Tong & Warhaft 1995). Earlier experiments by Sirivat & Warhaft (1982) indicated that the correlation between two scalars depends on their initial length scales. However, little is known about the behaviour of multi-scalar spectra in the spatial (wavenumber) domain, which is required for a quantitative description of the spectral mechanisms of differential diffusion. Furthermore, it appears that spectral transfer characteristics (as represented by triadic interactions) in the multi-scalar case have not been studied before.

In the study of differential diffusion, one is interested in joint statistical measures between different scalars. Yeung & Pope (1993) found that the correlation between the scalars has a strong scale dependence, and furthermore the evolution of the spectral coherency is determined directly by triadic interactions representing turbulent advection, with only an indirect influence of diffusivity differences. As an effect of molecular origin, differential diffusion is indeed observed to arise first at the small scales, but, in the absence of influences other than turbulent advection and molecular diffusion, is found to ultimately become important at the large scales as well (so that the scalars become completely de-correlated). In other words, from a spectral transfer point of view, differential diffusion can be thought of as an inverse cascade process in which incoherency propagates from the small scales to the large scales. Furthermore, one may expect different results if a coherent source of scalar fluctuations is present to counteract this inverse cascade. This is indeed the case if uniform mean scalar gradients are imposed, whereupon a quasi-steady non-zero asymptotic correlation coefficient between the scalars is maintained in time (Yeung & Moseley 1995*a*).

In this work, our primary objective is to investigate in detail the roles of different geometric classes of triadic interactions involving multiple scalars in the evolution of their coherency measured in Fourier space. More comprehensive results are first reported for single-scalar transfer at higher Reynolds number (R_λ up to 160), drawing upon a database at higher numerical resolution (up to 256^3 grid points in each realization) and including the effects of mean scalar gradients. The wider range of scales present in the new data allows us to distinguish between the effects of 'moderately' non-local triadic interactions and highly non-local ones. The dynamics of spectral coherency is then examined in detail. A primary issue is which triadic interactions tend to correlate the scalars (at specified scales), and which interactions tend to de-correlate them. Special attention is given, especially at early times, to the role of high-wavenumber velocity modes, although they are not active in

single-scalar transfer. The mean gradient (when present) contributions to coherency evolution are also documented. In nearly all cases ensemble averaging over multiple independent realizations have been performed (and are necessary) to ensure reliable results. Whereas in this paper we place a strong focus upon the spectral viewpoint, some information on spatial structure is also given.

The remainder of this paper is organized as follows. In §2 we give the basic equations defining spectral coherency and its evolution in time. In §3 we give a brief overview of the direct numerical simulations conducted including the spatial characteristics of the scalar fields, and summarize relevant facts from our recent work. The main results are presented in §4, including (*a*) further results on single-scalar transfer, and spectral coherency evolution (*b*) without mean scalar gradients and (*c*) in the presence of uniform mean scalar gradients. Conclusions are summarized in §5. Numerical issues concerning the extraction of spectral coherency from DNS data are addressed in the Appendix.

2. Spectral equations

We consider a set of passive scalars in constant-property turbulent flow, allowing for the presence of uniform mean scalar gradients. The transport equation for the fluctuation ϕ_α of each scalar (from its mean) with molecular diffusivity D_α is

$$\frac{\partial \phi_\alpha}{\partial t} + u_i \frac{\partial \phi_\alpha}{\partial x_i} = -u_i \frac{\partial \Phi_\alpha}{\partial x_i} + D_\alpha \frac{\partial^2 \phi_\alpha}{\partial x_i \partial x_i} , \tag{1}$$

where u_i is the velocity fluctuation, and the mean scalar field Φ_α is a prescribed linear function of the coordinates. (In this paper Greek subscripts designate individual scalars with different diffusivities, and are not subject to the summation convention.) In Fourier space, the contribution to the scalar variance from a Fourier mode $\boldsymbol{k}$ (with wavenumber magnitude k) may be written as $E^\phi_{\alpha\alpha}(\boldsymbol{k}) \equiv \langle \hat{\phi}_\alpha(\boldsymbol{k}) \hat{\phi}^*_\alpha(\boldsymbol{k}) \rangle$, where hats denote Fourier coefficients, asterisks denote complex conjugates, and angle brackets denote ensemble averages over multiple independent realizations. It is readily shown that $E^\phi_{\alpha\alpha}(\boldsymbol{k})$ evolves as

$$\frac{\partial E^\phi_{\alpha\alpha}(\boldsymbol{k})}{\partial t} = T^\phi_{\alpha\alpha}(\boldsymbol{k}) + G^\phi_{\alpha\alpha}(\boldsymbol{k}) - 2D_\alpha k^2 E^\phi_{\alpha\alpha}(\boldsymbol{k}) , \tag{2}$$

where the scalar transfer spectrum $T^\phi_{\alpha\alpha}(\boldsymbol{k})$ is given by

$$T^\phi_{\alpha\alpha}(\boldsymbol{k}) = 2\, k_j\, \mathrm{Im} \left[\left\langle \hat{\phi}^*_\alpha(\boldsymbol{k}) \int_{\boldsymbol{k}=\boldsymbol{p}+\boldsymbol{q}} \hat{u}_j(\boldsymbol{p}) \hat{\phi}_\alpha(\boldsymbol{q}) \mathrm{d}\boldsymbol{p} \right\rangle \right] , \tag{3}$$

and $G^\phi_{\alpha\alpha}(\boldsymbol{k})$ is proportional to the scalar flux spectrum, as

$$G^\phi_{\alpha\alpha}(\boldsymbol{k}) = -\frac{\partial \Phi_\alpha}{\partial x_i} \left[\hat{u}_i(\boldsymbol{k}) \hat{\phi}^*_\alpha(\boldsymbol{k}) + \hat{u}^*_i(\boldsymbol{k}) \hat{\phi}_\alpha(\boldsymbol{k}) \right] . \tag{4}$$

Advection of the scalar by the velocity fluctuations is represented in (3) as an integral over all triadic interactions coupling $\hat{\phi}_\alpha(\boldsymbol{k})$ with one velocity mode $\hat{u}_i(\boldsymbol{p})$ and another scalar mode $\hat{\phi}_\alpha(\boldsymbol{q})$, such that the wave-vectors $\boldsymbol{k}$, $\boldsymbol{p}$ and $\boldsymbol{q}$ form closed triangles in wavenumber space. In practice, the convolution integral in (3) is evaluated in a pseudo-spectral manner, so that the computational effort on an N^3 grid scales as

$N^3 \ln_2 N$. Spectral quantities are collected into discrete wavenumber shells, as

$$T^{\phi}_{\alpha\alpha}(k) \equiv \sum_{k-\frac{1}{2}\Delta k \leqslant |\boldsymbol{k}'| < k+\frac{1}{2}\Delta k} T^{\phi}_{\alpha\alpha}(\boldsymbol{k}') \equiv \sum_{\Delta k} T^{\phi}_{\alpha\alpha}(\boldsymbol{k}') \,, \tag{5}$$

where hereafter the notation $\sum_{\Delta k}$ is employed as a shorthand for summation over a shell of thickness Δk, usually taken to be unity. The transfer spectrum is readily decomposed into contributions from velocity and scalar modes in specified scale ranges. In particular, the detailed transfer function $T^{\phi}_{\alpha\alpha}(k|p,q)$ is the partial sum of the terms in (3) over those triads with the velocity mode in a range centred on p, and the other mode centred on q, where $\boldsymbol{p}$ and $\boldsymbol{q}$ are collected into discrete spherical shells in the same manner as in (5). Furthermore, the overall effects of velocity modes p and other scalar modes q are given respectively by the quantities

$$V^{\phi}_{\alpha\alpha}(k|p) = \sum_{q} T^{\phi}_{\alpha\alpha}(k|p,q) \,, \tag{6}$$

and

$$S^{\phi}_{\alpha\alpha}(k|q) = \sum_{p} T^{\phi}_{\alpha\alpha}(k|p,q) \,. \tag{7}$$

In the multi-scalar case, corresponding spectral equations for the co-spectrum $E^{\phi}_{\alpha\beta}(\boldsymbol{k}) \equiv \frac{1}{2}\langle \hat{\phi}_{\alpha}(\boldsymbol{k})\hat{\phi}^{*}_{\beta}(\boldsymbol{k}) + \hat{\phi}^{*}_{\alpha}(\boldsymbol{k})\hat{\phi}_{\beta}(\boldsymbol{k})\rangle$ at a Fourier mode $\boldsymbol{k}$ can be written (Yeung & Pope 1993). On the other hand, a more effective indicator of differential diffusion in Fourier space is a spectral correlation coefficient. This is formally given by the coherency spectrum, which is

$$\rho_{\alpha\beta}(\boldsymbol{k}) \equiv \frac{E^{\phi}_{\alpha\beta}(\boldsymbol{k})}{[E^{\phi}_{\alpha\alpha}(\boldsymbol{k})E^{\phi}_{\beta\beta}(\boldsymbol{k})]^{1/2}} \,. \tag{8}$$

Yeung & Pope (1993) derived an evolution equation for the coherency spectrum in the absence of mean scalar gradients, which contains only spectral transfer contributions without the explicit appearance of molecular diffusivities. Coherency development was represented in terms of spectra and co-spectra collected over discrete wavenumber shells. However, for reasons discussed in the Appendix, to study the roles of different classes of triadic interactions it is more appropriate, and convenient, to represent coherency by averaging over discrete Fourier modes in each shell. We define

$$\rho_{\alpha\beta}(\boldsymbol{k}) = \left\langle \frac{1}{M(k)} \sum_{\Delta k} r_{\alpha\beta}(\boldsymbol{k}') \right\rangle \,, \tag{9}$$

where $M(k)$ is the number of Fourier modes in a given shell, and $r_{\alpha\beta}$ at a given Fourier mode $\boldsymbol{k}$ is given by

$$r_{\alpha\beta}(\boldsymbol{k}) \equiv \frac{\frac{1}{2}(\hat{\phi}_{\alpha}\hat{\phi}^{*}_{\beta} + \hat{\phi}^{*}_{\alpha}\hat{\phi}_{\beta})}{|\hat{\phi}_{\alpha}|\,|\hat{\phi}_{\beta}|} \,. \tag{10}$$

The quantity $r_{\alpha\beta}(\boldsymbol{k})$ defined above has a useful alternative interpretation: namely (as is easily seen by writing the Fourier coefficients in polar form)

$$r_{\alpha\beta}(\boldsymbol{k}) = \cos[\theta_{\alpha}(\boldsymbol{k}) - \theta_{\beta}(\boldsymbol{k})] \,, \tag{11}$$

where θ_{α} and θ_{β} are the phase angles of $\hat{\phi}_{\alpha}(\boldsymbol{k})$ and $\hat{\phi}_{\beta}(\boldsymbol{k})$ in the complex plane. That is, the spectral coherency between different scalars is a measure of the phase alignment

between them in Fourier space. It is also seen from (11) that both $r_{\alpha\beta}(\boldsymbol{k})$, and hence $\rho_{\alpha\beta}(\boldsymbol{k})$, defined above, satisfy the Schwarz inequality required for correlation coefficients. Results on the statistics of phase alignment in Fourier space are included in §§4.2 and 4.3.

To present a coherency evolution equation consistent with the above definitions, we introduce some shorthand notation here. For example, we denote $\hat{\phi}_\alpha(\boldsymbol{k})\hat{\phi}^*_\alpha(\boldsymbol{k})$ by $e_{\alpha\alpha}(\boldsymbol{k})$, which gives the scalar spectral content at the mode $\boldsymbol{k}$ and whose ensemble average is just the scalar spectrum $E^\phi_{\alpha\alpha}(\boldsymbol{k})$. Similarly, we define the quantities $e_{\alpha\beta}(\boldsymbol{k})$, $t_{\alpha\alpha}(\boldsymbol{k})$, $t_{\alpha\beta}(\boldsymbol{k})$, etc., in relation to co-spectra and transfer spectra, and $f_{i\alpha}(\boldsymbol{k}) \equiv \frac{1}{2}[\hat{u}_i\hat{\phi}^*_\alpha + \hat{u}^*_i\hat{\phi}_\alpha]$ represents the corresponding contribution to the scalar flux spectrum. From the definition (10) and the Fourier transforms of (1) for scalars ϕ_α and ϕ_β an evolution equation for the quantity $r_{\alpha\beta}(\boldsymbol{k})$ may be derived. After some straightforward algebra, the result can be written as

$$\frac{\partial r_{\alpha\beta}(\boldsymbol{k})}{\partial t} = \left.\frac{\partial r_{\alpha\beta}(\boldsymbol{k})}{\partial t}\right|_{\mathrm{NL}} + m_{\alpha\beta}(\boldsymbol{k}) \,, \tag{12}$$

where the nonlinear transfer part is given by

$$\left.\frac{\partial r_{\alpha\beta}(\boldsymbol{k})}{\partial t}\right|_{\mathrm{NL}} = \left[e_{\alpha\alpha}e_{\beta\beta}\right]^{-3/2}\left[e_{\alpha\alpha}e_{\beta\beta}t_{\alpha\beta} - \tfrac{1}{2}e_{\alpha\alpha}e_{\alpha\beta}t_{\beta\beta} - \tfrac{1}{2}e_{\beta\beta}e_{\alpha\beta}t_{\alpha\alpha}\right] \,, \tag{13}$$

and the mean gradient term is

$$m_{\alpha\beta}(\boldsymbol{k}) = \left[e_{\alpha\alpha}e_{\beta\beta}\right]^{-3/2}\left[e_{\alpha\alpha}\frac{\partial \Phi_\beta}{\partial x_i}(e_{\alpha\beta}f_{i\beta} - e_{\beta\beta}f_{i\alpha}) + e_{\beta\beta}\frac{\partial \Phi_\alpha}{\partial x_i}(e_{\alpha\beta}f_{i\alpha} - e_{\alpha\alpha}f_{i\beta})\right] \,. \tag{14}$$

Finally, in view of relation (9), we define the *coherency evolution spectrum* within specified wavenumber shells with averaging over the modes in each shell as

$$h_{\alpha\beta}(k) = \frac{\partial \rho_{\alpha\beta}(k)}{\partial t} = \left\langle \frac{1}{M(k)}\sum_{\Delta k}\frac{\partial r_{\alpha\beta}(\boldsymbol{k}')}{\partial t}\right\rangle \,. \tag{15}$$

Taken together, relations (12) to (15) display a strong resemblance to (18) of Yeung & Pope (1993). Two differences are that (i) results are collected into wavenumber shells only at the last step, and (ii) the effects of production of scalar fluctuations by uniform mean gradients have been included. The absence of direct effects of molecular diffusivities is unchanged. For the mean gradient contributions, it should be noted that because the mean gradient term in (1) is linear, if (as in our calculations) scalar fluctuations are initially absent but generated directly by mean gradients, the effects of mean gradients on the correlation between the scalars are felt only through the alignment between the vectors $\nabla\Phi_\alpha$ and $\nabla\Phi_\beta$, but not their magnitudes (Yeung & Moseley 1995*a*). In this case we find that the magnitudes of the mean gradients ultimately cancel from the ratio in (14), as long as they are not zero.

A primary goal in this paper is to quantify the effects of different scales in the velocity and scalar fields on the evolution of coherency between different scalars at specified scale sizes. This may now be achieved in the framework of this Section by decomposing the spectral transfer terms in (13) into contributions from different classes of triadic interactions. For example, in analogy to $T^\phi_{\alpha\alpha}(k|p,q)$, we decompose the spectral transfer effects $h^{NL}_{\alpha\beta}(k)$ in $h_{\alpha\beta}(k)$ into contributions from triads with the velocity mode centred on p and the other scalar mode centred on q. That is,

$$h^{NL}_{\alpha\beta}(k) = \sum_{p,q} h^{NL}_{\alpha\beta}(k|p,q) \,, \tag{16}$$

and

$$h_{\alpha\beta}(k) = h_{\alpha\beta}^{NL}(k) + m_{\alpha\beta}(k) \,, \tag{17}$$

where $m_{\alpha\beta}(k)$ is obtained from $m_{\alpha\beta}(\boldsymbol{k})$ by averaging over Fourier modes in a given shell and over multiple realizations. We also denote by $h_{\alpha\beta}^{V}(k|p)$ and $h_{\alpha\beta}^{S}(k|q)$ respectively the overall effects of velocity and scalar modes through the transfer terms.

3. Simulation overview and scalar statistics

Direct numerical simulations of the exact three-dimensional time-dependent Navier–Stokes and passive scalar transport equations have been conducted using the pseudo-spectral algorithm of Rogallo (1981). Because we are interested in locality–non-locality issues in wavenumber space, for robust conclusions it is very desirable to have a wide range of scales present in the simulations. This provides strong motivation for achieving Reynolds numbers as high as current computational resources reasonably permit. In this work we have employed a massively parallel implementation (Yeung & Moseley 1995*b*) on an 512-node IBM SP that allows the use of more grid points by distributing memory among a large number of parallel processors.

Because we want to focus on the basic physics of the scalars, in this paper we consider the simplest turbulent flow possible: namely homogeneous isotropic turbulence which is furthermore made statistically stationary in time by numerical forcing of the large-scale motions, using the scheme of Eswaran & Pope (1988*a*). The highest Reynolds number reached in the present simulations is 160 based on the Taylor scale using a 256^3 grid, for which the wall-clock time per time step with three passive scalars and 64 parallel processors is only about 15 s. However, since multiple 256^3 simulations are still expensive, a significant fraction of the results in this paper are based on 128^3 data at $R_\lambda = 90$, with simulation parameters corresponding to those employed by Yeung & Pope (1989). The computational requirements are strongly associated with the need for multiple realizations over long time intervals: although a single 256^3 simulation (spanning 18 eddy-turnover times in this work) is well within our reach, to perform 20 such simulations (if physical conditions do not permit time averaging) is still, at present, too expensive. Indeed, computational cost has limited some recent 512^3 simulations (Jiménez *et al.* 1993; Wang *et al.* 1996) to relatively short periods of 2 eddy-turnover times or less.

The characteristics of the velocity and scalar fields in the simulations are summarized in tables 1 and 2, and in figure 1 which shows the energy and scalar spectra at Schmidt numbers (Sc) of 1/8, 1/4 and 1 in Kolmogorov scaling. The adequacy of numerical resolution in the velocity field is measured by the parameter $k_{max}\eta$, where k_{max} is the highest resolvable wavenumber on a given grid (allowing for alias error control), and η is the Kolmogorov length scale. The simulations satisfy the $k_{max}\eta \geqslant 1$ criterion proposed by Eswaran & Pope (1988*a*). However, in our attempt to reach higher Reynolds numbers, numerical resolution in the 256^3 case has been reduced somewhat compared to the 128^3 simulations. This is reflected in the turnups in the scaled energy spectra shown in figure 1 at the highest wavenumbers, and implies that some results at roughly the highest ten wavenumber shells should be treated with caution. Scale ratios in table 1 are formed from longitudinal integral length scale L_1, eddy-turnover time T_E ($\equiv L_1/u'$, where u' is the r.m.s. velocity fluctuation), and the Kolmogorov length and time scales (η, τ_η). It appears that the range of scales resolved is just wide enough to sustain a limited inertial range in the energy spectrum, indicated by a recognizable plateau in figure 1.

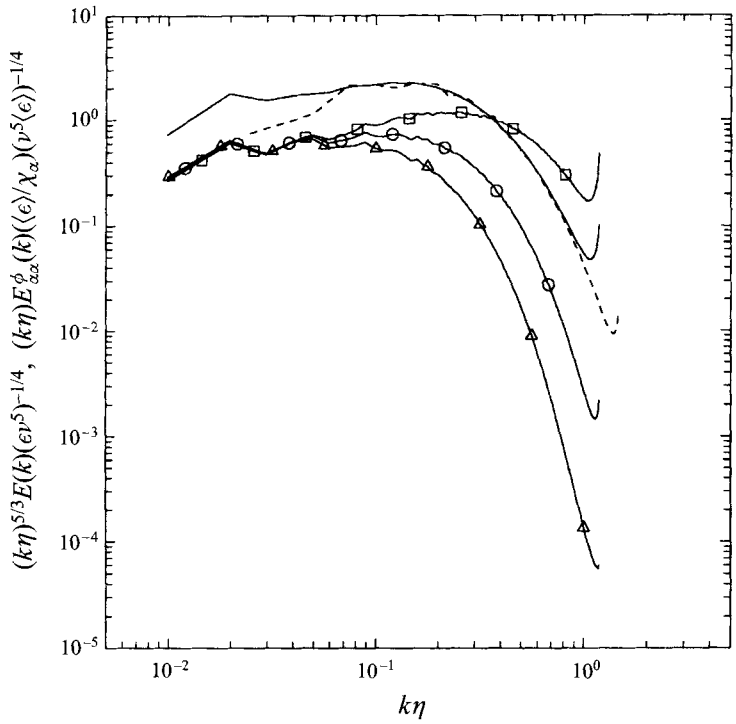

FIGURE 1. Time-averaged spectra scaled by the Kolmogorov variables, in $R_\lambda = 160$ (256^3) simulation, for energy (unmarked solid line) and scalars at Schmidt numbers 1/8 (△), 1/4 (○) and 1 (□) with uniform mean gradients; dashed line shows energy spectrum at $R_\lambda = 90$ (128^3) for comparison. An inertial range in the energy spectrum would be represented by a plateau at intermediate wavenumbers of height equalling the Kolmogorov constant. Here ϵ is the energy dissipation rate, ν is the kinematic viscosity, and χ_α is the dissipation of each scalar ϕ_α.

N	64	128	256
R_λ	38	90	160
k_{max}	30	60	120
$k_{max}\eta$	1.5	1.5	1.2
L_1/η	22	56	119
T_E/τ_η	7	12	19

TABLE 1. Numerical resolution and scale ratio information in the numerical simulations. Note that this paper reports 128^3 and 256^3 results, but information on 64^3 data in Yeung & Pope (1993) and Yeung (1994) is included for comparison.

It should be noted that the 256^3 velocity fields simulated in this paper are similar in Reynolds number and numerical resolution to that in Vincent & Meneguzzi (1991) ($R_\lambda = 150$ on a 240^3 grid), who used a different forcing scheme. On the other hand, Jiménez *et al.* (1993) performed highly resolved 256^3 simulations with $k_{max}\eta \approx 2$, but at lower Reynolds numbers. Their results also suggested that approximate inertial-range behaviour in the energy spectrum is possible for R_λ at 94 and higher. It can be estimated that in the case of an equilibrium axisymmetric turbulent jet, if the jet diameter is taken as a measure of the large scales and the turbulence intensity is 5%, an R_λ of 160 corresponds to a mean flow Reynolds number Re_d of about 34 000. This

	σ^2	μ_3	μ_4
$\nabla_\parallel\phi$, $Sc = 1/8$	21.98	1.892	14.02
$\nabla_\parallel\phi$, $Sc = 1/4$	44.55	1.896	16.08
$\nabla_\parallel\phi$, $Sc = 1$	178.5	1.328	14.72
$\nabla_\perp\phi$, $Sc = 1/8$	20.07	0.022	11.82
$\nabla_\perp\phi$, $Sc = 1/4$	40.88	0.018	13.57
$\nabla_\perp\phi$, $Sc = 1$	167.4	0.012	13.01

TABLE 2. Variance (σ^2), skewness (μ_3) and flatness (μ_4) factors for scalar gradient fluctuations parallel ($\nabla_\parallel\phi$) and perpendicular ($\nabla_\perp\phi$) to the mean gradient in the 256^3 $R_\lambda = 160$ simulation. The mean gradient is of unit magnitude.

is also comparable to the highest value of 64 000 reached in the mixing experiments of Smith (1994).

For scalar fields the Schmidt numbers are chosen to give the largest diffusivity ratio possible, subject to well-known numerical constraints. In figure 1 it may be seen that the scalar at $Sc = 1.0$ has considerable (more than the velocity field) high-wavenumber spectral content, so that its small scales are not very well resolved. Fortunately, as demonstrated in §4, this has only a limited impact on the behaviour of two-scalar triadic interactions involving high-wavenumber modes in this work. On the other hand, scalars of high diffusivity (or low Schmidt number) are dominated by the large scales, and consequently subjected to great statistical variability, since relatively few samples of the large scales exist in a solution domain of finite size.

In the absence of mean gradients or other production mechanisms, in stationary isotropic turbulence scalar fluctuations decay exponentially in a self-similar manner with a constant time scale (Eswaran & Pope 1988*b*). (It should be noted that in the case of *decaying* isotropic turbulence the time scale depends on length scales of the scalar field (Warhaft & Lumley 1978); the possibility of other similarity states has been studied Chasnov 1994.) Yeung & Pope (1993) found that, from identical-valued initial conditions, the scalars de-correlate rapidly at early times, especially at the small scales. However, beyond about two eddy-turnover times, differential diffusion becomes a very slow-evolving process, with large statistical variability. Nevertheless, the coherency spectrum indicates that ultimately all scales become completely de-correlated, effectively simultaneously in time.

When uniform mean gradients are present, scalar fluctuations are generated by velocity fluctuations acting across the mean gradient. If scalar fluctuations are initially absent, they become proportional to the mean gradient at all times. An approximate balance is reached between mean gradient production and molecular dissipation, so that the scalars become statistically stationary. (Such a stationary state is, however, not observed if the energy of the turbulence increases in time, for example in homogeneous turbulent shear flow (Rogers, Moin & Reynolds 1986).) Furthermore, a quasi-steady asymptotic correlation level is maintained (Yeung & Moseley 1995*a*), suggesting that the multi-scalar joint probability density functions also become stationary. This is very fortunate, because once stationarity is attained time averages may be taken from one realization without the need for many expensive simulations.

In all of our simulations, the probability density functions (PDFs) are found to be Gaussian. Other forms of the scalar PDF have been observed in isotropic turbulence: for instance, Jayesh & Warhaft (1992) found exponential tails in decaying grid-

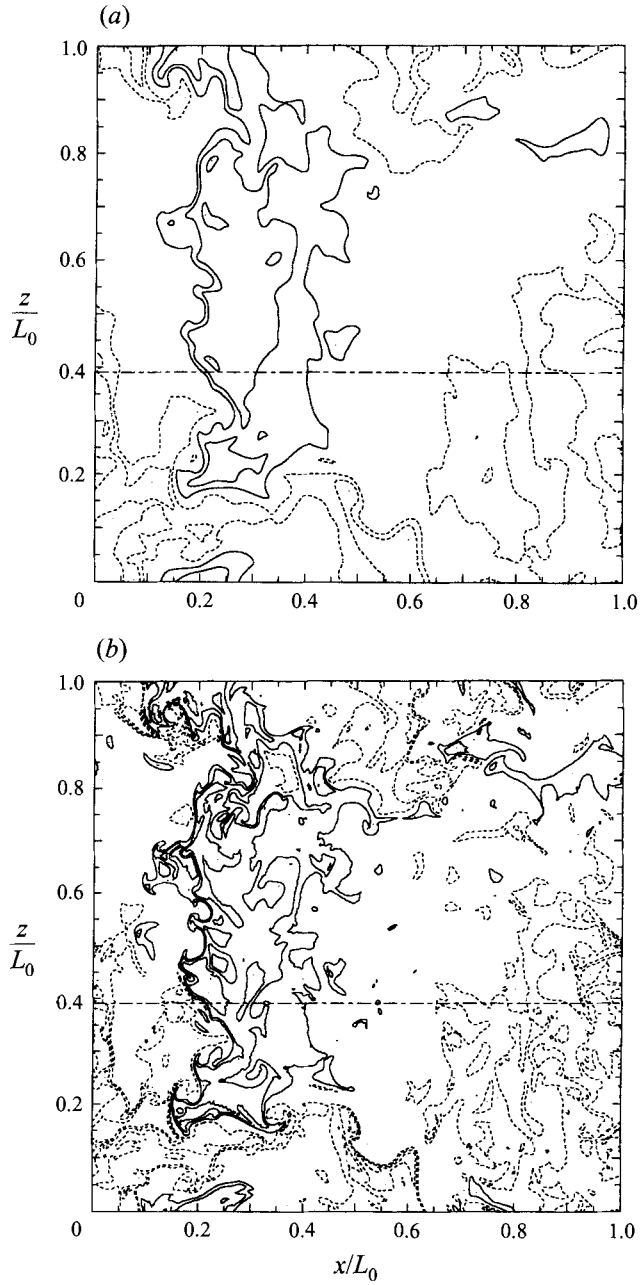

FIGURE 2. Contours of scalar fluctuations in a selected cross-sectional plane containing the mean scalar gradient vector, at $R_\lambda = 160$ for Schmidt numbers 1/8 (*a*) and 1 (*b*). Positive and negative contour levels are denoted by solid and dashed lines respectively, with the zero contour removed for clarity. The coordinates x (along the mean gradient direction) and z are scaled by the length of the solution domain ($L_0, = 2\pi$).

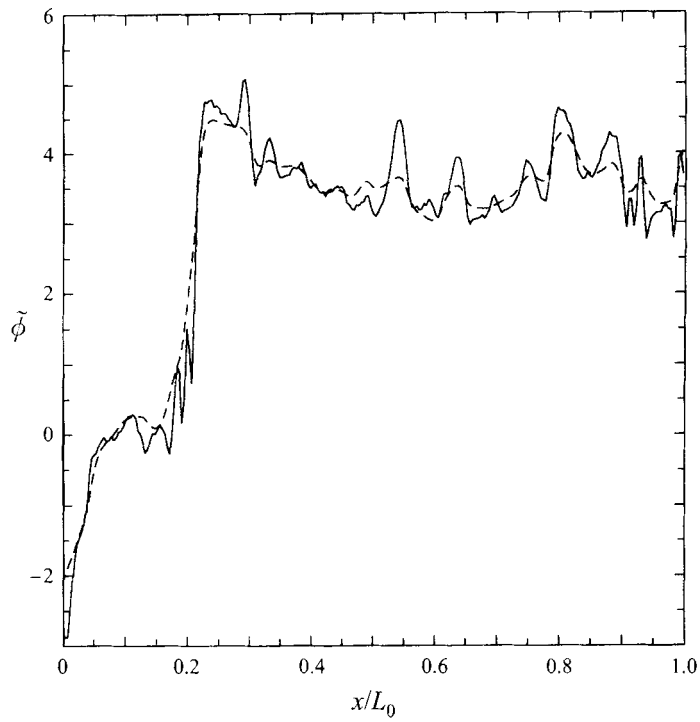

FIGURE 3. One-dimensional profiles of the total scalar field traversed in the direction of the mean gradient, across the position marked by the chain-dashed line in figure 2. Solid and dashed line represent scalars at $Sc = 1$ and $1/8$ respectively.

generated turbulence with an uniform transverse mean scalar gradient. However, in numerical simulations it is believed that such exponential tails occur only if the integral length scale of the turbulence is much smaller than the size of the solution domain (over which periodic boundary conditions are applied). This condition is not met in our simulations. The sensitivity of the form of the scalar PDF to initial conditions and properties of the velocity field has been investigated recently by Jaberi *et al.* (1995).

Statistical properties of intermittent scalar *gradient* fluctuations (with mean gradient) are similar to results given by Pumir (1994), both in the shape of the PDFs (not shown) and in the first few moments, which are listed in table 2. The 'parallel' component ($\nabla_{\parallel}\phi$) is positively skewed and more intermittent (with higher flatness factor) than the perpendicular component ($\nabla_{\perp}\phi$), which has a symmetric PDF. It is expected that measures of intermittency, including skewness and flatness, should increase with Schmidt number. The apparent departure of the scalar with $Sc = 1.0$ from this trend is because (due to limited resolution) its high-order moments are not well captured.

To complement the spectral emphasis in this paper, we discuss briefly the structure of scalar fluctuations in physical space in the case with mean gradients, using cross-sectional contours of the scalar fluctuations (figure 2*a*, *b*) and profiles taken in the direction of the mean gradient (figure 3). These results are very similar to those of Pumir (1994), with the new observation that the intermittent high-gradient regions for two highly correlated scalars (with correlation coefficient about 0.94) are indeed well correlated in space. The main difference between figures 2(*a*) and 2(*b*) is that, as

expected, steeper gradients are found for the less diffusive scalar. The profiles taken in figure 3 are of the total scalar field: that is, $\tilde{\phi} \equiv \phi + \nabla\Phi \cdot \boldsymbol{x}$. A cliff-like structure is seen at locations corresponding to the high-gradient regions in figures 2(*a*) and 2(*b*), consisting of a large jump in $\tilde{\phi}$ (caused by high gradient fluctuation) followed by a wide patch of lesser change in $\tilde{\phi}$ (due to negative scalar fluctuations). Steeper cliffs are observed for less-diffusive scalars.

The remarkable closeness between figures 2(*a*) and 2(*b*) suggests that the spatial structure of scalar fluctuations is largely dictated by the velocity field, independent of initial conditions and molecular diffusivity. To test this argument, we have performed some simulations in which the scalars are given nearly independent (and non-zero) initial conditions. It was found that the large-time asymptotic value of the two-scalar correlation is reached within about two eddy-turnover times. In other words, the velocity field essentially imposes a large-scale spatial organization on the scalars, although the small-scale features are modified by molecular diffusion.

The results reported by Yeung & Pope (1993) and Yeung & Moseley (1995*a*) have since been further substantiated by calculations at higher Reynolds numbers, and by the success of phenomenological models based on the DNS data (Yeung & Luo 1995). The spectral mechanisms of differential diffusion are investigated in this paper, through a detailed analysis of multi-scalar scale interactions.

4. Results and discussion

In the three subsections below, we present numerical results from analyses of DNS data concerning the detailed characteristics of single-scalar spectral transfer, and the role of multi-scalar triadic interactions in Fourier space for differential diffusion with and without uniform mean gradients. The physical questions addressed include the following:

First, what are the effects of the presence of a wider range of scales and mean gradient production on the spectral transfer of single scalars at different Schmidt numbers? Second, what types of triadic interactions are responsible for the rapid de-correlation observed at early times observed in differential diffusion? Third, when the coherency becomes stationary or slow-changing, what is the nature of the balance of processes tending to increase or decrease the coherency at various scales? Finally, does mean gradient production provide a strong direct contribution to coherency evolution, and/or indirectly modify the spectral transfer contributions so that a quasi-steady state is attained?

4.1. *Further results on single-scalar transfer*

Some brief DNS results on single-scalar transfer were previously given in Yeung (1994), for a scalar at $Sc = 1.0$ in self-similar decay in stationary isotropic turbulence at $R_\lambda = 38$ simulated with 64^3 grid points. We present below more detailed data at higher Reynolds numbers with a wide range of scales, including the effects of mean gradients and different Schmidt numbers.

Figure 4 shows, via the transfer function $V_{\alpha\alpha}^{\phi}(k|p)$, the contributions of velocity modes at different scales to the spectral transfer of a scalar at $Sc = 1.0$ without mean gradients, at $R_\lambda = 90$ on an 128^3 grid. In performing ensemble averaging (with 34 realizations) we note that when the scalar fields are in a self-similar state, the shape of the scalar spectrum is statistically the same over time and between different realizations. This implies that only the shapes (rather than absolute magnitudes) of the spectral transfer functions are of interest. Accordingly, the scalar fluctuations

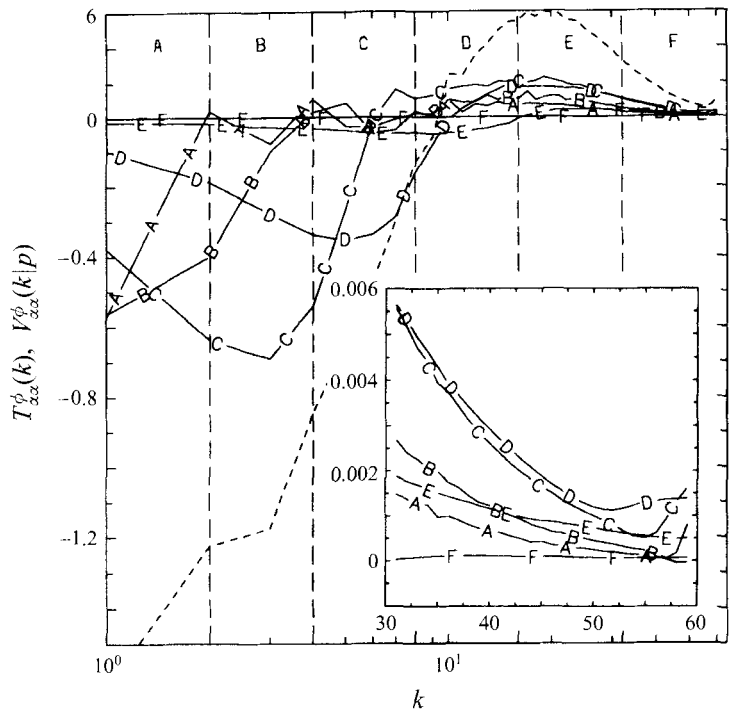

FIGURE 4. Decomposition of the scalar transfer spectrum function $T^{\phi}_{\alpha\alpha}(k)$ (dashed line) into contributions $V^{\phi}_{\alpha\alpha}(k|p)$ from velocity modes p in the logarithmically spaced ranges A–F, for a scalar with $Sc = 1.0$ and no mean gradient in 128^3 simulations at $R_\lambda = 90$. The highest resolved wavenumber is 60 and the Kolmogorov wavenumber $1/\eta$ is 39.5. The inset shows the high-wavenumber part magnified.

in each realization are scaled to yield the same variance (taken to be unity for convenience).

The overall transfer represented by the dashed line in figure 4 is, as expected, from the large scales (low wavenumbers) to the small scales (high wavenumbers). It may also be seen, more clearly in the inset, that at high wavenumbers (range F, $k \geqslant 32$) the largest contributions come from triads with velocity modes in the ranges C and D ($4 \leqslant p < 16$). In this sense the dominant interactions are non-local, with a scale ratio of about 4 to 16 between the velocity and scalar modes. It should be noted, however, that the effects of the most highly non-local, or 'distant' interactions (with p in the ranges A and B) on the high-wavenumber modes are considerably weaker. Another striking observation is that spectral transfer caused by the velocity modes in the highest wavenumber band (range F) is virtually negligible.

The relative strengths of couplings with different ranges of velocity modes require physical explanation. The process of forward spectral transfer represents the creation of scalar fluctuations at smaller scales as a result of advection by the velocity field. Such an effect would be weak if the velocity fluctuations have little energy (at the small scales), or if they are nearly uniform in space (at the largest scales) – in which case a blob of scalar would experience little deformation as it is transported in a bodily manner. Consequently, the most efficient spectral transfer at the small scales would be due to velocity modes that have both significant energy and dissipation. In the results of Yeung (1994) the range of scales was rather limited, such that the

peaks of the energy and dissipation spectra were separated only by a ratio of 2, and the two dominant velocity wavenumber bands ($2 \leqslant p < 4$ and $4 \leqslant p < 8$) together contained 71% of the energy as well as 63% of the dissipation. However, in the present 128^3 results at $R_\lambda = 90$ the spectral peaks are separated by a ratio of 7, and the strongest bands are $4 \leqslant p < 8$ and $8 \leqslant p < 16$, which now together contain only 28% of the energy but 59% of the dissipation. This comparison suggests that at high Reynolds numbers – extrapolated beyond the range of our simulations – the strongest contributions to spectral transfer will come from velocity scales in the neighbourhood of the peak of the dissipation spectrum (rather than the peak of the energy spectrum). Because this peak will still occur at a scale considerably larger than the Kolmogorov scale, at high wavenumbers these interactions are still expected to be moderately non-local. The dominance of moderately non-local interactions is also observed in 256^3 data at $R_\lambda = 160$ with uniform mean scalar gradients.

To characterize the spectral transfer in greater detail, we show in figure 5(*a–c*), for the same dataset in figure 4, the detailed triadic transfer contributions $T^\phi_{\alpha\alpha}(k|p,q)$ to $V^\phi_{\alpha\alpha}(k|p)$ for p in three different ranges (note the different plotting scales). In all three cases, and especially when $p \leqslant q$, we observe forward cascade behaviour, with the detailed transfers changing sign at the mid-point of the q interval, from negative (removal) when $q > k$ to positive (addition) when $k > q$. The intensity and magnitude of the net effect, however, depend on the scale size of the velocity mode. For the largest eddies ($1 \leqslant p < 2$), there is nearly complete mutual cancellation between scalar transfers from the next larger scale range and to the next smaller scale range. The curves appear narrow at high wavenumbers because, for low p and large k, the triangle inequality restricts q to within a narrow range close to k.

In figure 5(*c*) it may be seen that, when relatively high-wavenumber velocity modes are considered (in this case $16 \leqslant p < 32$), the primary contributions at high wavenumbers are associated with triads where the other scalar mode q is also at high wavenumber. This indicates that local interactions at high wavenumbers are stronger than those that couple two scalar modes of disparate scales by a high-wavenumber velocity mode. However, as discussed above, transfer by small-scale velocity fluctuations is much smaller in magnitude than the effect of velocity modes near the peak of the dissipation spectrum.

The results of Yeung (1994) indicated that the interaction between scalar modes is primarily a local forward cascade process in favour of the generation of smaller-scale scalar fluctuations. This conclusion is supported by the transfer function $S^\phi_{\alpha\alpha}(k|q)$ for the 128^3 data at $R_\lambda = 90$, shown in figure 6. These curves are distinguished by their spiky nature (which indicates localness of transfer), and their sign change in the middle of the q interval (which is consistent with a forward cascade). The behaviour of $S^\phi_{\alpha\alpha}(k|q)$ also appears to be statistically robust, with little of the jitter apparent in the $V^\phi_{\alpha\alpha}(k|p)$ data shown in figure 4. The only scalar modes that do not receive any significant input from the others are those at the top of the cascade: there the lowest-wavenumber modes (range A) primarily lose their spectral content to modes in ranges B and C.

For a given range of scalar modes, the velocity modes that contribute the most to the forward cascade can be identified by plotting, for a given range of q, the contributions $T^\phi_{\alpha\alpha}(k|p,q)$ from different ranges of p to $S^\phi_{\alpha\alpha}(k|q)$. Such plots (not shown) also suggest a dominant role of velocity modes near the peak of the dissipation spectrum, consistent with the discussions based on figures 4 and 5 above.

A limitation in the interpretation of the triadic transfers $T^\phi_{\alpha\alpha}(k|p,q)$ (and especially the associated quantities $V^\phi_{\alpha\alpha}(k|p)$, $S^\phi_{\alpha\alpha}(k|q)$) is that, because k, p and q are all grouped

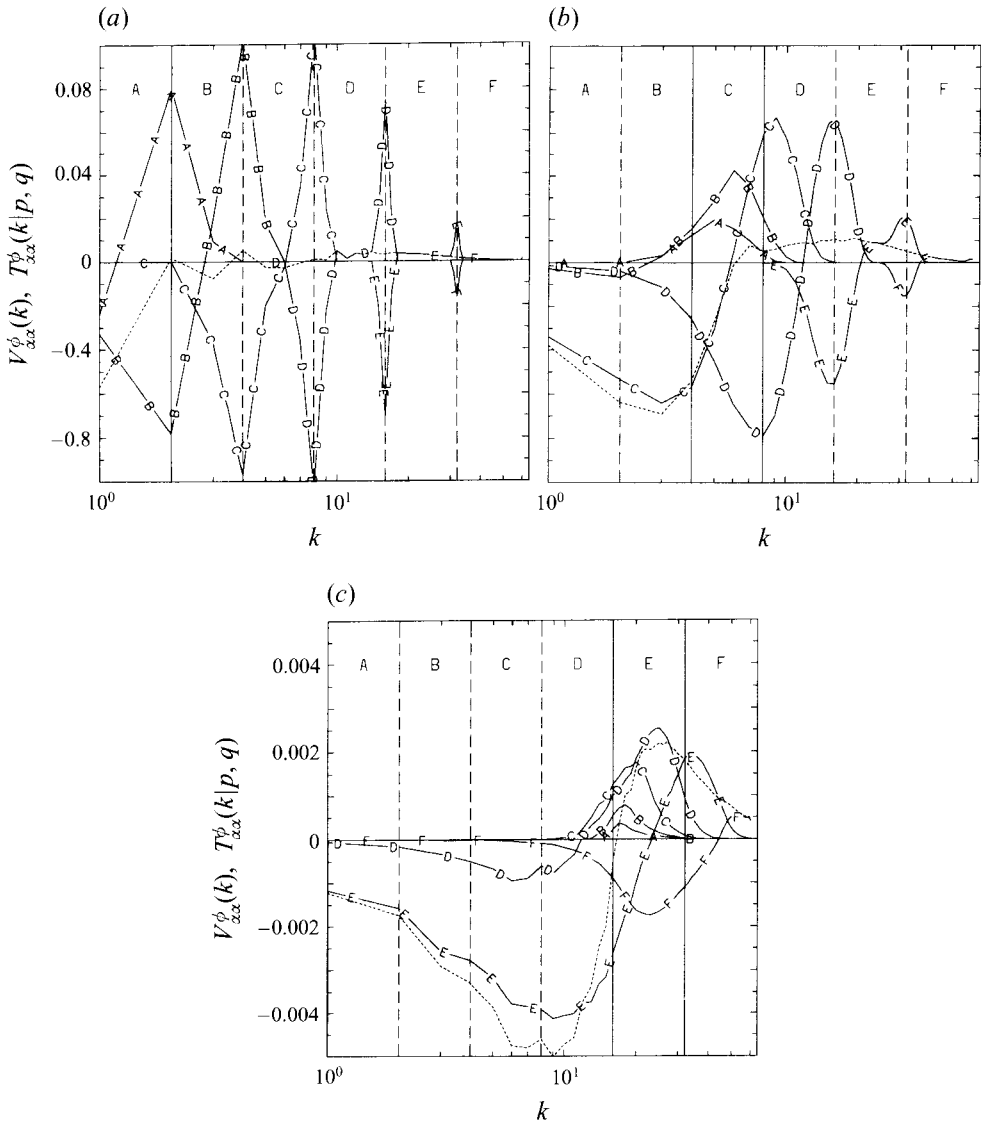

FIGURE 5. Decomposition of the velocity mode transfer function $V^{\phi}_{\alpha\alpha}(k|p)$ (dashed line) for selected ranges of p in the data of figure 4: (*a*) $1 \leqslant p < 2$ (range A), (*b*) $4 \leqslant p < 8$ (range C) and (*c*) $16 \leqslant p < 32$ (range E) into detailed transfer $T^{\phi}_{\alpha\alpha}(k|p,q)$ contributions from scalar modes q in the logarithmically spaced ranges A–F. Note that the scales in (*c*) are magnified.

into shells of finite thickness, not all triads within a given $T^{\phi}_{\alpha\alpha}(k|p,q)$ have the same scale separation. In other words, these quantities only provide indirect information on the degree of scale disparity within the triads. To address this shortcoming we adopt here as a direct measure of scale disparity the parameter s introduced by Zhou (1993*a*, *b*), which is the ratio between the longest and shortest legs in a triad:

$$s \equiv \frac{\max(k', p', q')}{\min(k', p', q')} \,. \tag{18}$$

The triadic interactions can then be re-grouped according to the disparity amongst

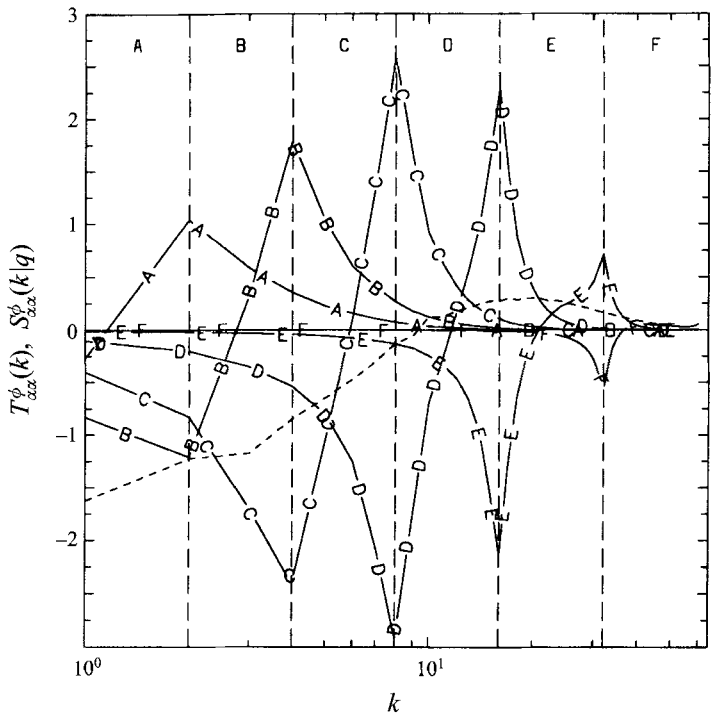

FIGURE 6. Decomposition of the scalar transfer spectrum function $T^{\phi}_{\alpha\alpha}(k)$ (dashed line) into contributions $S^{\phi}_{\alpha\alpha}(k|q)$ from scalar modes q in the logarithmically spaced ranges A–F (for the data of figure 4).

the interacting scales in each triad as

$$T^{\phi}_{\alpha\alpha}(k,s) = \sum_{\Delta k} \sum_{p',q'|s} t_{\alpha\alpha}(\boldsymbol{k}',\boldsymbol{p}',\boldsymbol{q}') \,, \tag{19}$$

where $t_{\alpha\alpha}(\boldsymbol{k}'\boldsymbol{p}',\boldsymbol{q}')$ represents the effect of a single triad (with $\boldsymbol{k}'+\boldsymbol{p}'+\boldsymbol{q}'=0$) on the scalar mode $\boldsymbol{k}'$.

The scale disparity parameter s has been used successfully in energy transfer studies to complement information derived from triadic interactions (Zhou, Yeung & Brasseur 1996). Its use for scalar fields carries some ambiguity, since in principle it does not distinguish (for instance) between non-local triads in which the velocity mode is the shortest leg and those in which the shortest leg is a scalar mode. This is not a great difficulty, since we have already established that these two types of non-local triads behave very differently – for example, triads with a high-wavenumber velocity mode contribute very little to scalar transfer. More limiting, in practice, is the fact that unlike the triadic transfers $T^{\phi}_{\alpha\alpha}(k|p,q)$ which can be calculated efficiently in a pseudo-spectral manner, the calculation of $T^{\phi}_{\alpha\alpha}(k,s)$ requires a direct and time-consuming summation for the convolution integral in (3). In effect, a discrete summation must be carried out explicitly over all possible triads, which are classified according to their value of the parameter s, as written in (19). Since two legs of a triangle can be freely chosen, the number of triads, and hence CPU cost on an N^3 grid, scales as N^6. The total number of triads is found to be 6.9 billion when $N = 64$. In our case, the need for multiple realizations compounds the difficulty.

Although the computation of $T^{\phi}_{\alpha\alpha}(k,s)$ is, for the reasons given above, very difficult,

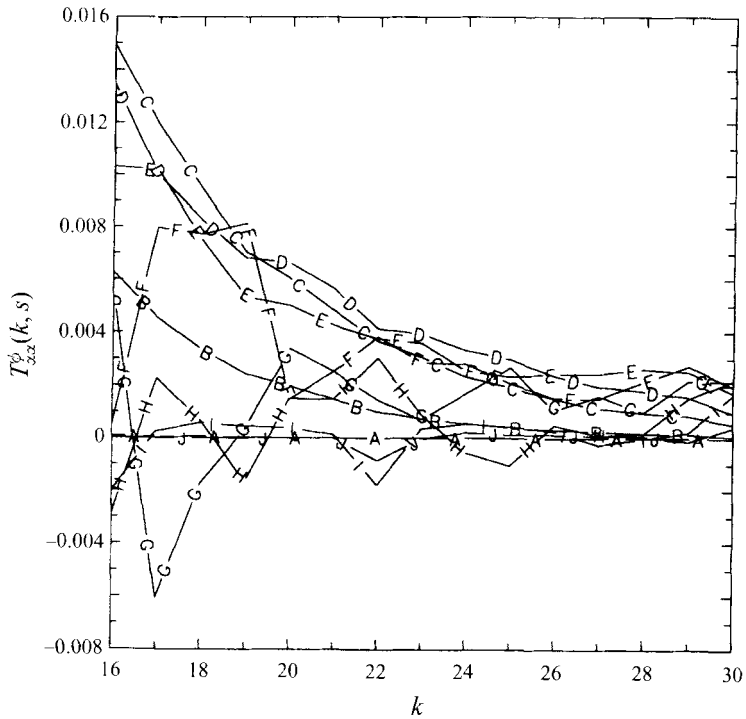

FIGURE 7. Spectral transfer function $T^{\phi}_{\chi\chi}(k,s)$ for different half-octaves ($1 \leqslant s < \sqrt{2}$, ... $16\sqrt{2} \leqslant s < 32$) of the scale disparity parameter s, for a scalar with $Sc = 1.0$ in 64^3 simulations at $R_\lambda = 38$.

we have nevertheless performed such calculations on a (coarser) 64^3 grid at $R_\lambda = 38$, for the conditions of Yeung (1994). Averages from 11 realizations are shown in figure 7, for wavenumbers in the highest octave simulated (where the net transfer is primarily positive). Despite the significant statistical jitter, it may be seen that triads of both very low (curve A) and very high (curves H, I) scale disparity contribute little to the spectral transfer. For a wide range of wavenumbers the dominant interactions have a scale separation between 2 and $4\sqrt{2} \approx 5.6$. At higher wavenumbers the role of interactions with higher scale disparity increases somewhat, which reflects the action of the same group of velocity modes on scalar modes of increasing wavenumber. Overall, the $T^{\phi}_{\chi\alpha}(k,s)$ information obtained broadly confirms deductions drawn from the behaviour of triadic transfers.

With the $R_\lambda = 90$ results at $Sc = 1.0$ without mean gradients as reference, we now present additional results to illustrate the effects of uniform mean gradients, as well as different Reynolds and Schmidt numbers, on the spectral transfer between scalar modes. When uniform mean gradients are imposed, attainment of a stationary state in the scalar field permits time averaging of the transfer spectra calculated from Fourier coefficients saved at regular time intervals within the simulations. Figure 8 shows the scalar transfer $S^{\phi}_{\chi\alpha}(k|q)$ at the same Reynolds and Schmidt numbers as before, but with uniform mean gradients. The scalar variances have also been normalized to unity. Clearly, the basic conclusion of a local forward cascade remains unchanged. The most noticeable difference between figures 6 and 8 is that the spikes at lower wavenumbers in the latter have increased strength relative to those at high wavenumbers. This is the result of a scalar spectrum that itself has more low-wavenumber content, such that

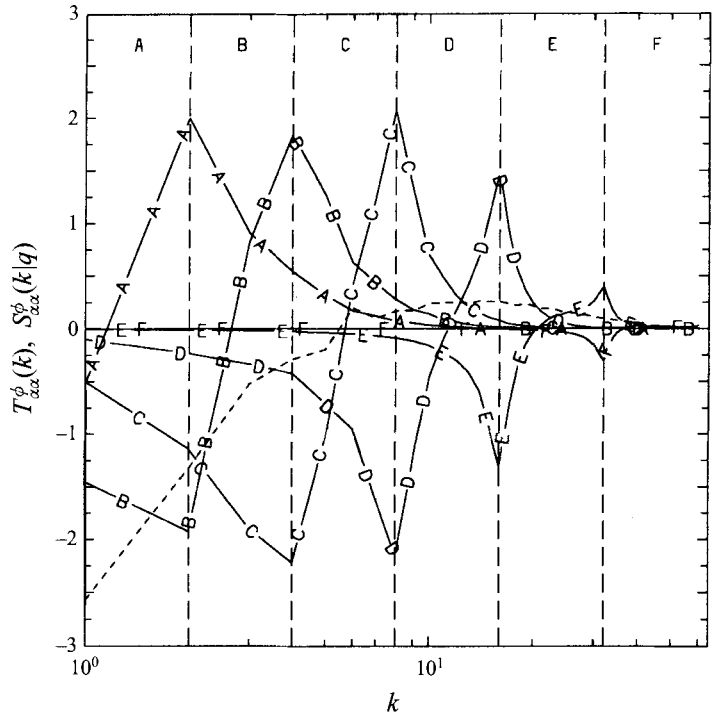

FIGURE 8. Same as figure 6, but in the stationary state maintained by uniform mean scalar gradients.

there is more scalar 'energy' available for transfer from the largest scales. These largest scales are maintained by mean gradient production through the scalar flux spectrum, which is heavily concentrated at the lowest wavenumbers because the energy of the flow is, in turn, maintained by forcing at the large scales.

Figure 9 shows the scalar transfer at $R_\lambda = 160$, from a 256^3 simulation with mean gradients. At this Reynolds number the energy spectrum (see figure 1) has a recognizable, though limited, inertial range. However, the spectral transfer results appear very similar to those in figure 8 at $R_\lambda = 90$, except that the cascade now extends to the highest wavenumbers that are present on the 256^3 grid. The greater scale separation accompanying the increase in Reynolds number does cause a shift in the size of the dominant velocity modes coupling the scalar modes, in the manner discussed with reference to figure 4 earlier in this section. Because of statistical variability, quantitative statements on the velocity mode contributions $V^{\phi}_{\alpha\alpha}(k|p)$ (not shown) require more realizations or a longer period for time averaging.

The effects of Schmidt number are shown via the scalar transfer at $Sc = 1/8$ in figure 10, with the velocity field being the same as in figure 9. At this low Schmidt number the scalar field has, of course, a narrower range of scales, and in fact has more low-wavenumber content than the velocity field. Because of this spectral distribution, the transfer is most active at the large scales, tapering off quickly as higher wavenumbers are approached.

All results in this subsection indicate a robust local forward cascade behaviour in which the scale size of the most active velocity modes varies with Reynolds number. Multi-scalar transfer characteristics are studied in the next two subsections.

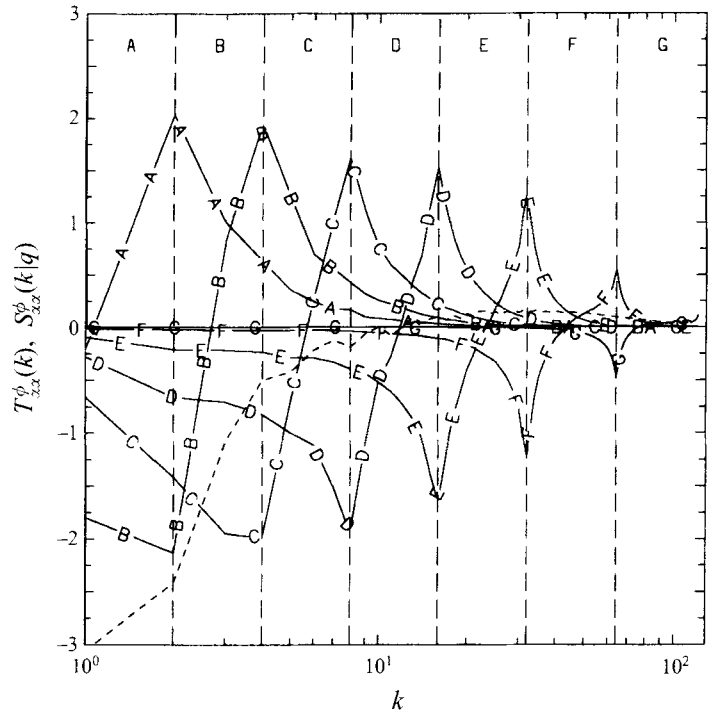

FIGURE 9. Same as figure 8, but in a 256^3 simulation at $R_\lambda = 160$.

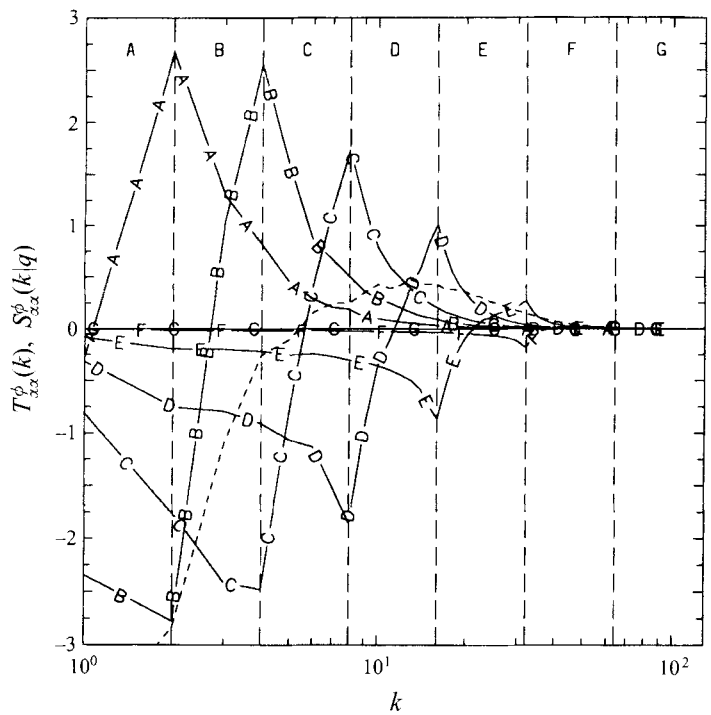

FIGURE 10. Same as figure 9, but for a scalar with Schmidt number 1/8.

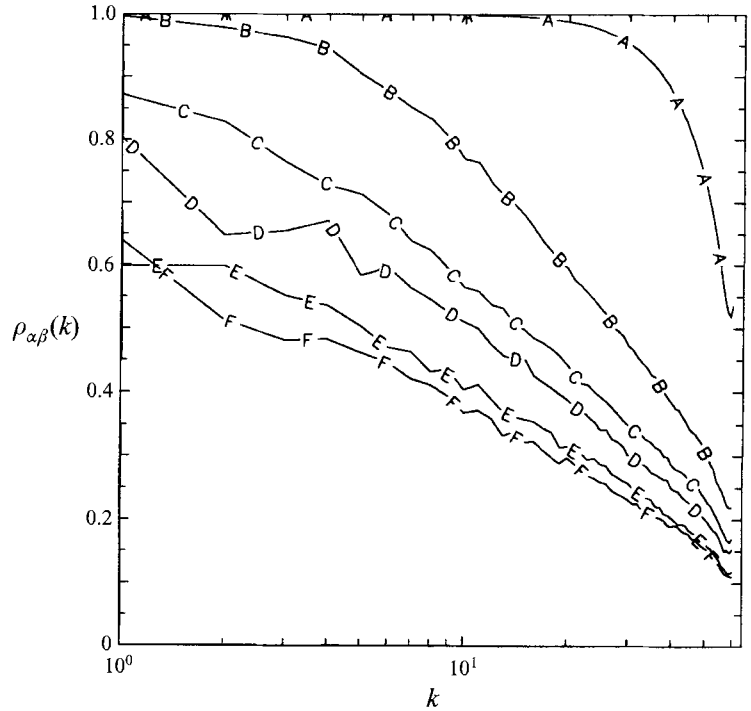

FIGURE 11. Coherency spectrum for scalars with $Sc = 1/8$ and 1 at different times in 128^3 simulations at $R_\lambda = 90$ without mean scalar gradient. Lines A to F are respectively at $t/T_E = 0.042$, 0.708, 5.66, 10.38, 15.09, and 19.81. For reference, the ratio between T_E and τ_η is 11.8.

4.2. *Coherency evolution without mean gradients*

In differential diffusion without mean scalar gradients, it has been shown previously (Yeung & Pope 1993) that spectral transfer is directly responsible for the evolution of spectral coherency between scalars of different molecular diffusivities. We present below results on the evolution of coherency for 128^3 simulations in stationary isotropic turbulence at $R_\lambda = 90$, for three scalars at Schmidt numbers 1/8, 1/4 and 1 without mean scalar gradients. This is followed by an examination of the roles of different classes of triadic interactions in differential diffusion at different times. Except where stated otherwise, in each realization the scalars evolve from identical-valued initial conditions, being made equal to an instantaneous self-similar scalar field with $Sc = 1.0$.

Figure 11 shows the coherency (defined as in (9)) between scalars at $Sc = 1/8$ and 1 at different times, with data averaged over 14 realizations. Although the results differ quantitatively from the coherency spectrum used previously (see Appendix), the qualitative behaviour is the same as in the lower Reynolds number data of Yeung & Pope (1993). At early times the scalars become de-correlated very rapidly at the small scales. At later times the large scales de-correlate steadily. Although, because of computational expense, the new simulations (spanning 20 eddy-turnover times) are not long enough to achieve an asymptotic state, they do support the conclusion (Yeung & Pope 1993) that the scalars ultimately become completely de-correlated at all scales simultaneously. The statistical jitter seen at low wavenumbers is due to sampling limitations.

As indicated in §2, spectral coherency may be represented (through (9) and (11))

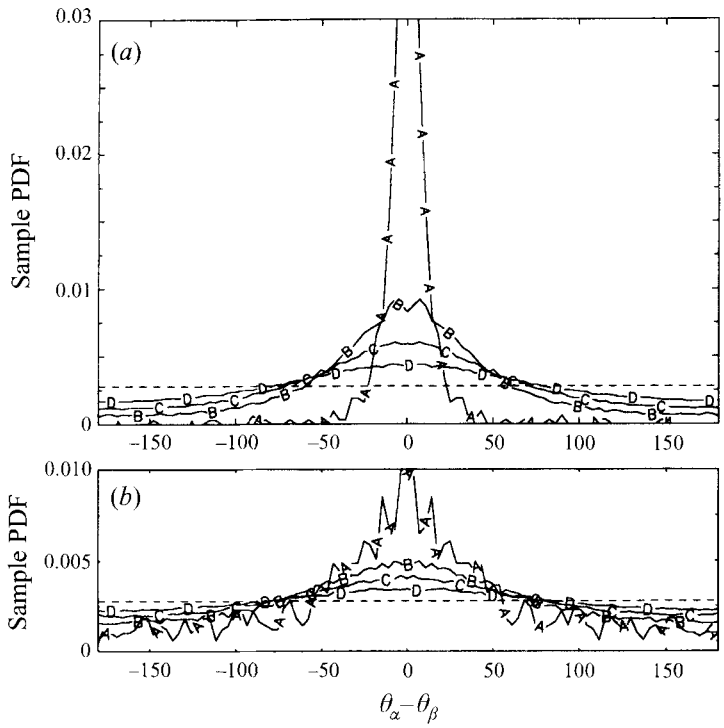

FIGURE 12. Sample PDFs of the difference in phase angle between scalars with $Sc = 1/8$ and 1 in Fourier space, for unit-thickness wavenumber shells centred on $k = 3$, 21, 39, 57 respectively (lines A to D). The data are extracted from 128^3 simulations at $R_\lambda = 90$ without mean scalar gradient at (*a*) $t/T_E = 0.708$ and (*b*) $t/T_E = 19.81$. The dashed line indicates a uniform distribution.

by the phase difference between two scalars in Fourier space, averaged over Fourier modes in specified wavenumber shells. Within each shell the probability distributions of the phase angles of each scalar, and the difference between them, can be estimated from the DNS data. In all cases we find that the phase angle of each scalar, considered separately (as θ_α, θ_β, etc.), is uniformly distributed. This is because the real and imaginary parts of $\hat{\phi}_\alpha(\boldsymbol{k})$ can be viewed as, respectively, the Fourier cosine and sine transforms of the even and odd parts of the scalar fluctuation field as a function of the coordinates in physical space. Since sines and cosines are recoverable from each other by a simple shifting in physical space, and that in homogeneous turbulence such shifting is statistically immaterial, in our simulations the real and imaginary parts have essentially the same physical meaning and statistical properties. This implies that there is no net tendency for the scalar Fourier coefficient $\hat{\phi}_\alpha(\boldsymbol{k})$ to be aligned (in the complex plane) relative to its real or imaginary parts in any particular way, so that the angle $\theta_\alpha(\boldsymbol{k})$ must be uniformly distributed.

In the two-scalar case, a high value of the coherency may be associated with small phase angles between the scalars, and as they become less correlated over time the phase difference can be expected to increase on average. The sample probability density function (PDF) of the phase angle between scalars at $Sc = 1/8$ and 1 is shown in figure 12 at 0.708 and 19.81 eddy-turnover times, corresponding to the coherency data (lines A and E) averaged over spectral shells in figure 11. The phase difference is taken in the principal branch $-\pi \leqslant \theta_\alpha - \theta_\beta < \pi$ (but expressed in degrees in the figures). These PDFs are perfectly symmetric because of the conjugate symmetry

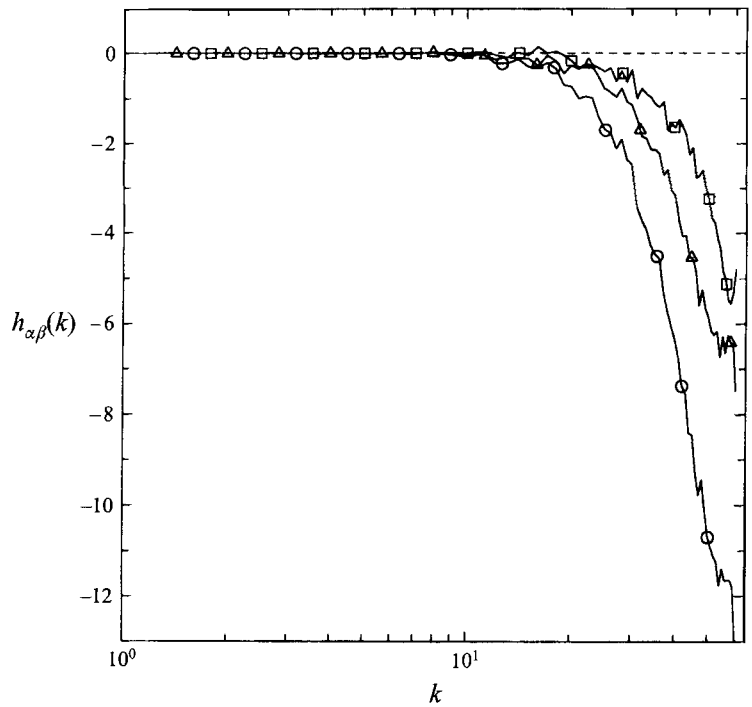

FIGURE 13. The coherency evolution spectrum $h_{\alpha\beta}(k)$ for scalars at an early stage of differential diffusion (t/T_E=0.042, or $t/\tau_\eta = 0.5$) in 128^3 simulations at $R_\lambda = 90$ without mean scalar gradient. Three pairs of scalars are shown, with Schmidt numbers (1/8, 1/4) (△), (1/8, 1) (○), and (1/4, 1) (□).

property of Fourier modes: for any given $\hat{\phi}_\alpha(\boldsymbol{k})$, there exists a $\hat{\phi}_\alpha(-\boldsymbol{k}) = \hat{\phi}^*_\alpha(\boldsymbol{k})$ with a phase angle of exactly the same magnitude but opposite in sign. Large statistical variability is, again, evident in the low-wavenumber shells which contain relatively few Fourier modes.

At early times it may be seen from figure 12(*a*) that for low-wavenumber shells this phase angle PDF is narrow and sharply peaked at the origin, reflecting high coherency. At higher wavenumbers the PDFs are progressively wider and flatter, with increased probabilities for large phase differences. A spreading towards larger phase differences over time is also evident when comparing figures 12(*a*) and 12(*b*). It may be readily demonstrated that the phase difference between two completely uncorrelated and Gaussian distributed scalars takes on a uniform distribution, since then because of statistical independence there can be no preferential orientation of each scalar relative to the other. Consequently, the limiting state for the PDFs shown at asymptotically large times is a uniform distribution, given by the horizontal dashed line in the scales shown. This asymptote has not yet been reached at end of the simulation (20 eddy-turnover times), when the coherency for the highest wavenumber shell shown is about 0.125.

It is clearly important to understand the processes responsible for the rapid decorrelation rate observed at the small scales at early times, which we investigate by studying the behaviour of the coherency evolution spectrum (15). To ensure an adequate ensemble size, we have performed a series of short-time simulations which allow us to capture the early-time phenomena at low computational cost. The coherency evolution spectra $h_{\alpha\beta}(k)$ averaged from 34 realizations for three pairs of

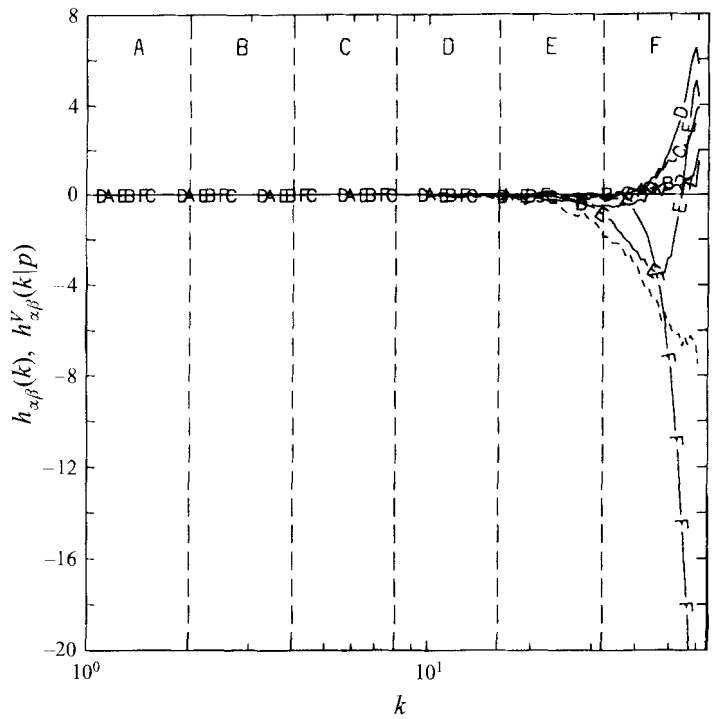

FIGURE 14. Decomposition of the coherency evolution spectrum $h_{\alpha\beta}(k)$ (dashed line) into contributions $h^V_{\alpha\beta}(k|p)$ from velocity modes in logarithmically spaced ranges A–F, for a pair of scalars with $Sc = 1/8$ and 1 at an early stage of differential diffusion (t/T_E=0.042, or $t/\tau_\eta = 0.5$) without mean gradient in 128^3 simulations at $R_\lambda = 90$.

scalars are shown in figure 13, at about 0.5 Kolmogorov time scales (τ_η) after they begin to evolve from identical-valued initial conditions. It is clear that at this time the scalars are de-correlating rapidly at the small scales, whereas the effects of differential diffusion have yet to reach the large scales. The de-correlation rate is largest in magnitude for the pair of scalars with $Sc = 1/8$ and 1.

In figure 13 it may be seen that at time $t/\tau_\eta = 0.5$ the $Sc = (1/4,\ 1)$ pair of scalars has a weaker instantaneous de-correlation rate than the $Sc = (1/8,\ 1/4)$ pair, although the former has a largest diffusivity ratio. As pointed out by a referee, this behaviour is a direct consequence of the diffusivity difference (which is larger for the latter pair) appearing as a factor in the source term in the transport equation for the mean-squared diffusivity difference (e.g. in Bilger & Dibble 1982). This source term dominates the dynamics of rapid de-correlation at early times, but becomes unimportant at later stages.

An analysis given by Yeung & Pope (1993) indicates that the rate of de-correlation from identical initial conditions at early times (less than one Kolmogorov time scale) increases with the relative high-wavenumber content (expressed by a shape parameter) in the initial scalar spectrum. The effects of the choice of initial spectrum have been studied by performing a separate series of short-time simulations in which the scalars are initially made equal to a self-similar field with $Sc = 1/8$. In this case the initial spectrum has less high-wavenumber content than one with $Sc = 1.0$. Whereas many similarities are found, the de-correlation rates at early times are, as expected, less

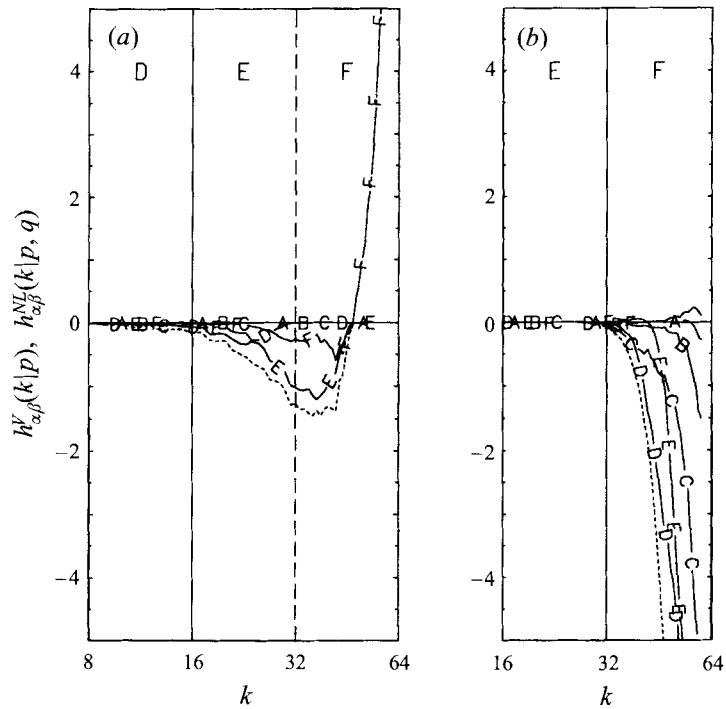

FIGURE 15. Decomposition of the velocity-mode contribution $h^V_{\alpha\beta}(k|p)$ (dashed line) to the coherency evolution spectrum for selected ranges of p in the data of figure 14: (*a*) $8 \leqslant p < 16$ (range D) and (*b*) $32 \leqslant p < 64$ (range F), into detailed contributions $h^{NL}_{\alpha\beta}(k|p,q)$ from scalar modes q in the logarithmically spaced ranges A–F. The data are essentially zero at wavenumbers lower than the range shown.

than in the data of figure 13. In addition, statistical variability is increased when the initial scalar spectrum has more low-wavenumber content.

We now consider the contributions of different ranges of velocity and scalar modes to the coherency evolution spectra shown in figure 13, for scalars with $Sc = 1/8$ and 1, without the mean gradient term in (17). Figure 14 shows the contributions of velocity modes, as $h^V_{\alpha\beta}(k|p)$. The interesting processes occur primarily at the small scales in the scalar fields. It may be seen that the largest scales (ranges A and B) in the velocity field contribute very little, whereas intermediate scales (ranges C and D) tend to promote coherency, and that the smallest scales (ranges E and F) tend to decrease coherency. The intermediate scales in the velocity field have been shown (see §4.1) to be strongly associated with the forward cascade in the scalar fields towards the high wavenumbers. Consequently, we may conclude that the forward cascade is coherent. This is a reasonable result because the spectral cascade extracts scalar fluctuations from lower wavenumbers, where the scalars are more strongly correlated, so that this spectral flux tends to make the scalars at higher wavenumber more coherent. Because the spectra of the scalars decrease with wavenumber, this spectral flux causes only a relatively small fractional rate of decrease of coherency at low wavenumbers, but a larger fractional rate of increase at high wavenumbers. This leads to the observation that, for intermediate values of p, $h^V_{\alpha\beta}(k|p)$ has relatively shallow negative troughs but high positive peaks.

Although it was established in §4.1 that high-wavenumber velocity modes contribute

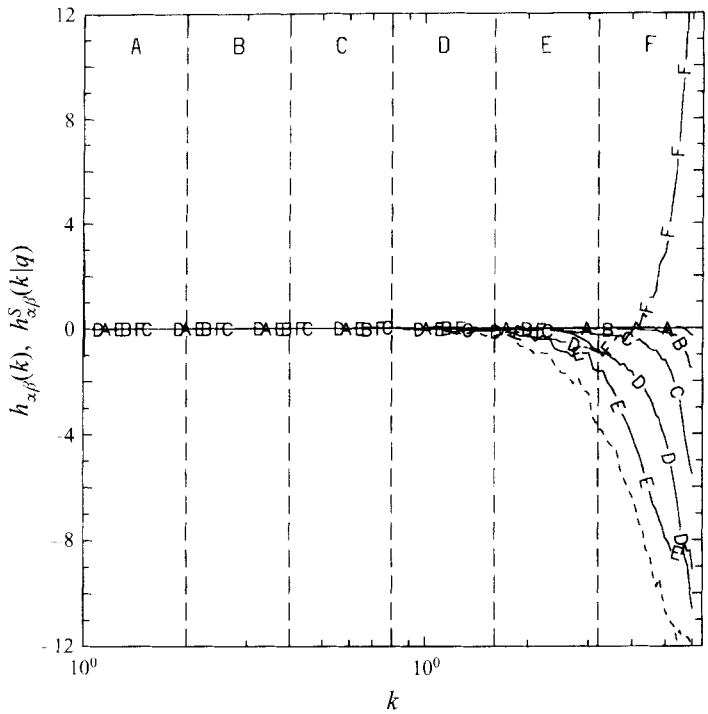

FIGURE 16. Decomposition of the coherency evolution spectrum $h_{\alpha\beta}(k)$ (dashed line) into contributions $h^S_{\alpha\beta}(k|q)$ from scalar modes q in the logarithmic ranges A–F (for the data of figure 14).

very little to spectral transfer, it is seen in figure 14 that these modes are primarily responsible for rapid de-correlation between the scalars at the small scales. It is noteworthy that line F ($32 \leqslant p < 64$) begins to be significantly negative at roughly the mid-point of the interval $32 \leqslant k < 64$ (in this case, mainly for p in the higher half of the interval F). This suggests that the de-correlating effect is associated with triads in which both k and p are at high wavenumber, but with the further constraint that $p < k$. Velocity modes in range E show behaviour intermediate between those in ranges D and F. They are de-correlating for wavenumbers k within a ratio of about 2 from the mid-point of range E, but show a coherent forward cascade effect at yet higher values of k.

It is already clear from the observations above that the relative scale difference between velocity and scalar modes plays a pivotal role in determining whether the former tend to promote or reduce coherency. It may also be seen that for all ranges of p, $h^V_{\alpha\beta}(k|p)$ deviates appreciably from zero only when the wavenumber k is at least as high as the lower end of the p range. In other words, triads in which the velocity mode is the longest leg ($k, q < p$) have virtually no effect on the coherency development of the scalar modes forming the shorter legs.

As in the case of single-scalar transfer, it is useful to examine the 'detailed' contributions $h^{NL}_{\alpha\beta}(k|p,q)$ from different ranges of scalar modes q to the quantity $h^V_{\alpha\beta}(k|p)$ for the ranges of p that are most active in coherency evolution. Figure 15 shows such detailed breakdowns for velocity modes p in the octaves (*a*) $8 \leqslant p < 16$ and (*b*) $32 \leqslant p < 64$. For velocity modes in the range $8 \leqslant p < 16$, the coherent forward cascade at high-wavenumbers is seen to be associated with high wavenumber scalar

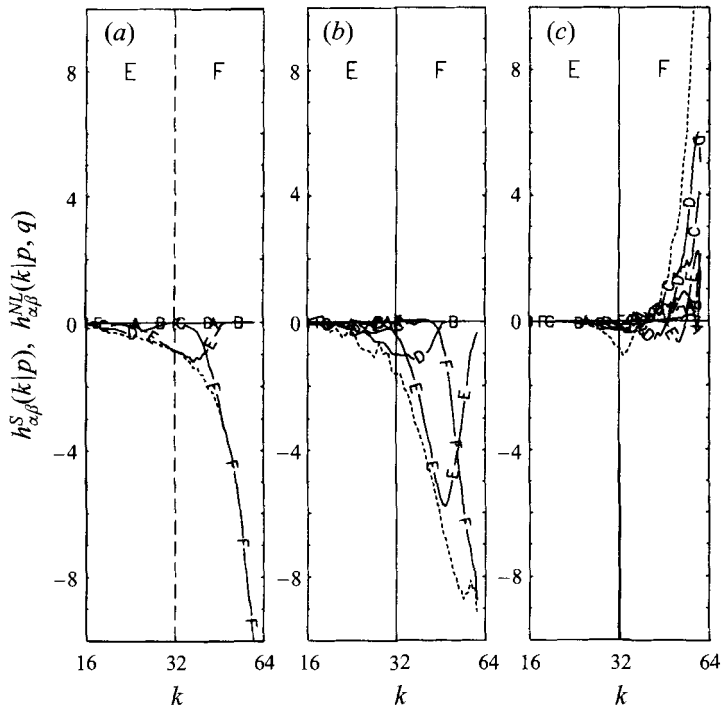

FIGURE 17. Decomposition of the scalar-mode contribution $h^S_{\alpha\beta}(k|q)$ (dashed line) to the coherency evolution spectrum for selected ranges of q in the data of figure 14: (*a*) $8 \leqslant q < 16$ (range D), (*b*) $16 \leqslant q < 32$ (range E) and (*c*) $32 \leqslant q < 64$ (range F) into detailed contributions $h^{NL}_{\alpha\beta}(k|p,q)$ from velocity modes p in the logarithmically spaced ranges A–F. The data are essentially zero at wavenumbers lower than the range shown.

modes (ranges E and F). This is consistent with the cascade being of the nature of local transfer by moderately non-local interactions. On the other hand, for velocity modes in the range $32 \leqslant p < 64$, the de-correlating contributions are seen to be strongly associated with scalar modes of lower, although not much lower, wavenumber. In other words, the most strongly de-correlating triads are local between velocity and scalar modes, but moderately non-local within scalar modes. Furthermore, together with the condition $p < k$ deduced from figure 14, these local triads have the property $q < p < k$. That is, the velocity mode is intermediate in scale between two scalar modes. One interpretation of this result is that in these triads the velocity mode has qualitatively different effects on the two scalar modes, and so tend to affect them in ways that make the scalar modes (carrying different scalars) develop spectral content different from each other. Fully local triads where all three modes are at high wavenumber (curve F in figure 15*b*, hardly different from zero) without appreciable scale separation are found to have no significant effect on coherency evolution (nor, as seen in §4.1, any significant role in spectral transfer).

The relative roles of scalar modes in coherency evolution are shown by a plot of the quantity $h^S_{\alpha\beta}(k|q)$ in figure 16. Again, interest is primarily in the effects on high-wavenumber modes. A forward cascade contribution is seen from scalar modes q in the range F, which is strongly coherent for the smallest scales. De-correlating effects are observed for other scalar modes of lower wavenumber, and are particu-

larly strong (curve E) when the scale separation between the scalar modes is only moderate.

For a more complete description, we compare in figure 17(*a–c*) the contributions $h^{NL}_{\alpha\beta}(k|p,q)$ from different ranges of the velocity modes p to $h^{S}_{\alpha\beta}(k|q)$ for scalar modes q in the ranges that contribute most to coherency evolution. The dominant effect of intermediate-wavenumber scalar modes on the smallest scales is de-correlating. Consistent with the role suggested for triads of the type $q < p < k$ above, the magnitude of line F in figure 17(*a*) increases rapidly when k increases past the mid-point of range F. For triads with $16 \leqslant p,q < 32$ (curve E in figure 17*b*) as the wavenumber k and hence scale separation is increased, an upturn in $h^{NL}_{\alpha\beta}(k|p,q)$ is observed at $k \approx 45$. This upturn marks the scale separation between velocity and scalar modes beyond which some triads begin to exhibit coherent forward cascade behaviour. Finally, in figure 17(*c*) it is seen that when the scalar modes are local relative to each other, a coherent forward cascade is the dominant process at high wavenumbers.

The physical picture discussed above for coherency evolution at early times is that in which a coherent forward cascade is more than offset by a strong de-correlating tendency from moderately non-local triads in which the velocity mode is intermediate in scale between two scalar modes, so that the net result (as observed) is rapid de-correlation at the small scales. At large times, the observation that coherency evolves much more slowly (ultimately becoming quasi-steady) indicates that the different processes involved in coherency evolution become approximately in balance. The magnitude and spectral extent of both coherent and incoherent processes are also expected to be different from early times, because of the changes in the shapes of the scalar spectra and co-spectra that have occurred. However, because of greatly increased statistical variability, the details of coherency evolution at large times are much more difficult to determine with accuracy.

Figures 18 and 19 show the contributions $h^{V}_{\alpha\beta}(k|p)$ and $h^{S}_{\alpha\beta}(k|q)$ to the coherency evolution spectrum $h_{\alpha\beta}(k)$ at 20 eddy-turnover times (after 8000 time steps) from 14 realizations. The statistical jitter present is of a degree much greater than that observed at early times. Nevertheless, significant differences with the early-time results (figures 14 and 16) are evident. It may be seen that the net coherency evolution spectrum is now nearly flat on average, with small ensemble-averaged values within about ± 0.5 at all scales (in contrast with -13 at the highest wavenumbers at early times in figure 13). Whereas high-wavenumber velocity modes (range F) are still strongly de-correlating, they are now nearly counter-balanced by the combined coherent forward cascade effects of intermediate-scale velocity modes. In addition, coherent cascade effects are now no longer restricted to the smallest scales, but are felt over a wider wavenumber range. The effect of velocity modes $16 \leqslant p < 32$ (range E) on scalar modes $32 \leqslant k < 64$ (range F) is now primarily coherent.

The increased importance of local forward cascade effects between scalar modes on the evolution of coherency at later times is also evident in figure 19. This forward cascade is now observable at intermediate as well as high wavenumbers. Both the correlating and de-correlating processes in coherency evolution may be considered to 'propagate' in time from the small scales to the large scales, in an 'inverse cascade' manner. It is important to note that at later times the coherency spectrum has a definite negative slope over a wide range of wavenumbers. As a consequence, even at relatively low wavenumbers the forward spectral flux carries the scalars from a more coherent wavenumber range to a less coherent one, thereby tending to maintain the coherency at higher wavenumbers or at least reduce its rate of decrease.

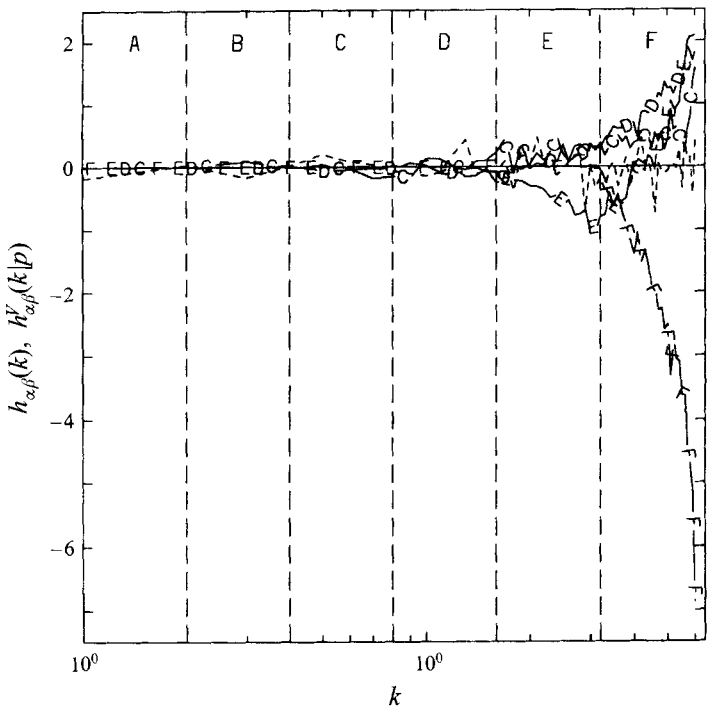

FIGURE 18. Same as figure 14, but at a later time in differential diffusion ($t/T_E = 19.81$), from 14 realizations. To reduce clutter, small contributions from ranges A and B have been omitted.

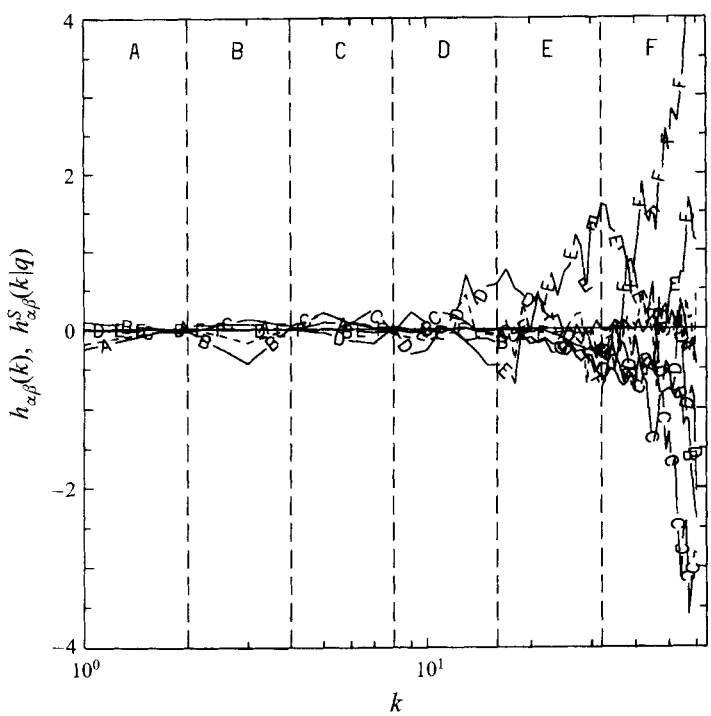

FIGURE 19. Same as figure 16, but at a later time in differential diffusion ($t/T_E = 19.81$), from 14 realizations.

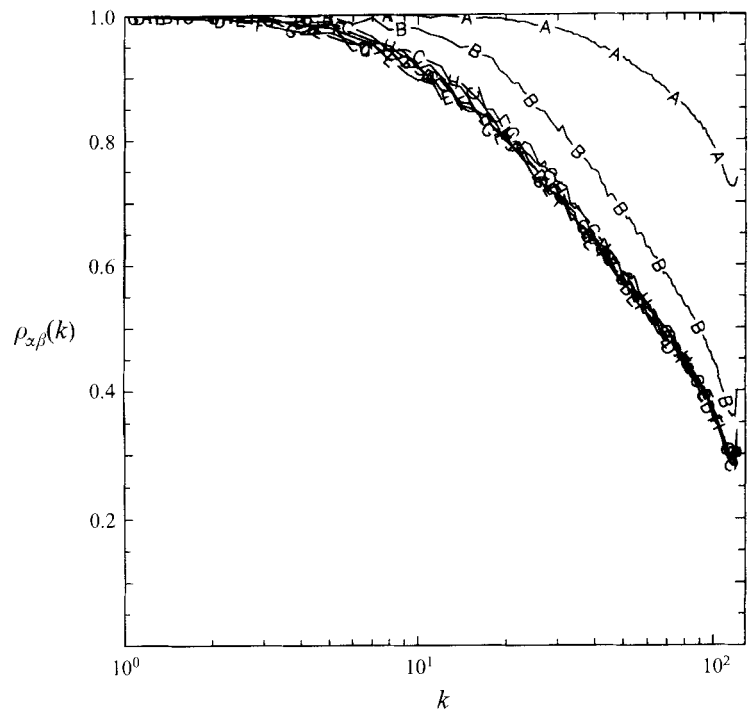

FIGURE 20. Coherency spectrum for scalars with $Sc = 1/8$ and 1 at different times in a 256^3 simulation at $R_\lambda = 160$ with uniform mean scalar gradients. Lines A to H are respectively at $t/T_E = 0.128$, 0.640, 1.921, 5.122, 8.323, 11.5, 14.53 and 17.41. For reference, the ratio T_E/τ_η is 18.77.

On the other hand, de-correlating triads of the type $q < p < k$ will have an appreciable impact only if the velocity mode p acts between two scalar modes of significantly different coherency. At later times, because the coherency spectrum is less steep, a significant difference in coherency between scalar modes k and q requires a greater scale separation between them. That is, for a given k such interactions are appreciable only for q at relatively low wavenumbers. As seen in figure 19, the largest negative contributions to $h_{\alpha\beta}(k)$ at the high wavenumbers are now due to scalar modes in the range $4 \leqslant q < 8$ (range C), which are at considerably lower wavenumber than the most dominant range $16 \leqslant q < 32$ seen in the early-time results. In other words, the most actively de-correlating triadic interactions become more non-local between scalar modes with increasing time.

The results of this subsection indicate that non-local interactions between scalar modes coupled by a velocity mode of intermediate scale are primarily responsible for the propagation of incoherency from the small scales to the large scales, although at later times this process is ultimately balanced by a local coherent forward cascade from the large scales to the small scales. It is natural to expect that this spectral picture, and hence the gross characteristics of differential diffusion, to be altered if a source of scalar fluctuations is present, in a manner that depends on its spectral content. The effects of such a source caused by a uniform mean scalar gradient are examined in the next subsection.

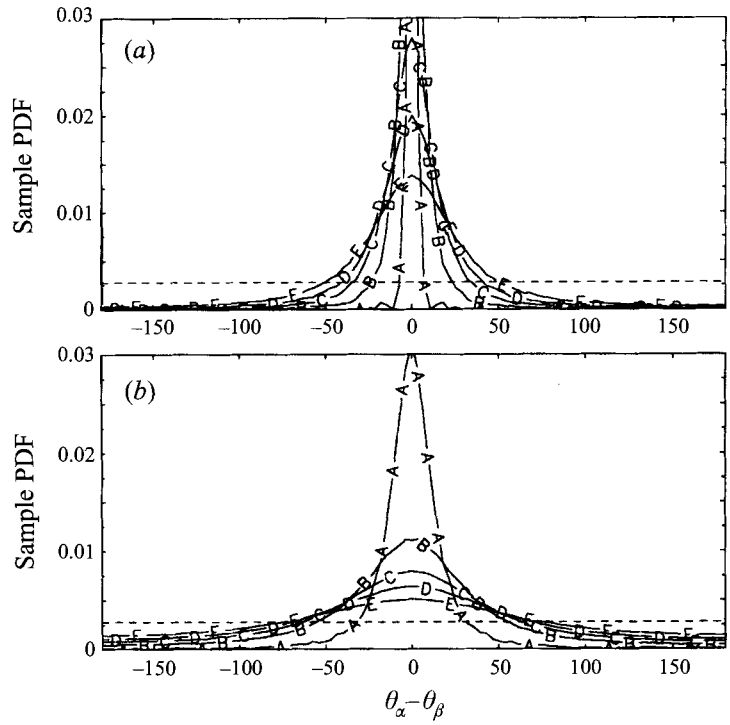

FIGURE 21. Sample PDFs of the difference in phase angle between scalars at $Sc = 1/8$ and 1, for wavenumber shells centered on $k = 10$, 35, 60, 85, and 110 respectively (lines A–E). The data are taken from the 256^3 $R_\lambda = 160$ simulation with uniform mean scalar gradients at (*a*) $t/T_E = 0.128$ and (*b*) averaged over t/T_E from 1.921 to 18.57. The dashed line indicates a uniform distribution.

4.3. *Coherency evolution with uniform mean gradients*

As mentioned before, when uniform mean scalar gradients are imposed, the scalar fluctuations attain a statistically stationary state in which their joint correlation coefficients are maintained at quasi-steady asymptotic values. Higher-resolution DNS data can be more conveniently obtained in this case, because stationarity permits time-averaging of spectral transfer characteristics from just one sufficiently long simulation. We present below a detailed characterization of coherency evolution with mean scalar gradient, through the analysis of DNS data at $R_\lambda = 160$ and 90 on 256^3 and 128^3 grids respectively. The 256^3 simulation spanned about 18.6 eddy-turnover times (with 15 000 time steps, consuming about 63 CPU hours on each of 64 parallel processors). Three scalar fields at Schmidt numbers 1/8, 1/4 and 1 with the same uniform mean gradient (taken to be unity) were simulated. However, most of the results given below pertain to the pair with $Sc = 1/8$ and 1, which display the strongest effects of differential diffusion.

The spectral coherency between the scalars at $Sc = 1/8$ and 1 at different times in the 256^3 simulation is shown in figure 20. The turnups at the high-wavenumber end are symptomatic of imperfect numerical resolution (see §3), but fortunately are significant only in roughly the highest 10 wavenumber shells on the 256^3 grid (i.e. for $k > 110$). It is clearly seen that, consistent with the attainment of a quasi-steady correlation coefficient, the coherency spectrum also becomes quasi-steady – after only about 1.9 eddy-turnover times. This observation allows spectral transfer characteristics, including coherency evolution, to be averaged over time from 1.9

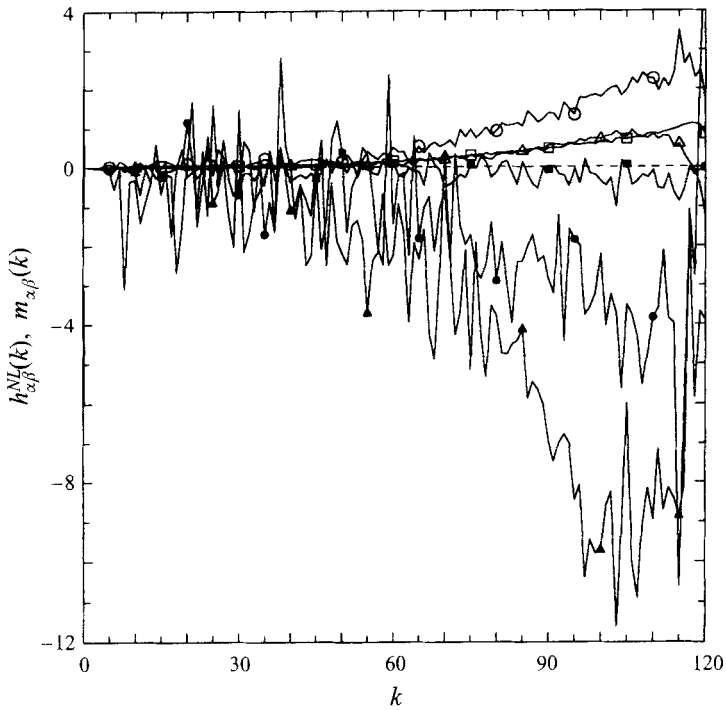

FIGURE 22. Comparison of spectral transfer and mean gradient contributions to coherency contribution, $h^{NL}_{\alpha\beta}(k)$ (open symbols) versus $m_{\alpha\beta}(k)$ (closed symbols) for scalars with $Sc = 1/8$ and 1 in 256^3 $R_\lambda = 160$ simulation with uniform mean scalar gradients. The data are shown for times t/T_E at 0.128 (triangles), 0.640 (circles) and averaged from 1.921 to 18.57 (squares).

to 18.6 eddy-turnover times (until the end of the simulation). In contrast with results without mean gradients (figure 11), it is seen that the largest scales remain almost perfectly correlated at all times. In other words, effects of differential diffusion originating from the high-wavenumber end now fail to reach the lowest wavenumbers. Further analysis below shows that this is due to the presence of a coherent source of scalar fluctuations, as well as a strengthened forward cascade counteracting the inverse cascade of incoherency propagation from the small scales.

The results of figure 20 suggest that in Fourier space the scalars remain largely in phase with each other at the low wavenumbers. The distributions of their phase (angle) difference within selected wavenumber shells at early and later times are shown in figure 21(*a*, *b*). At the early time of $t/\tau_\eta = 2.4$ (or $t/T_E = 0.128$, corresponding to line A in figure 20), these distributions are clearly sharply peaked. At later times (figure 21*b*), where we have performed time averaging as discussed above, at low wavenumbers this distribution is still heavily concentrated around zero. At higher wavenumbers the phase difference distribution becomes more spread out, but, unlike the case of no mean scalar gradients, it does not approach the uniform distribution that would result if the scalars were to become completely de-correlated (and independent).

To understand how the presence of mean gradients causes a quasi-steady coherency spectrum to be maintained, we study both the direct mean-gradient contribution $m_{\alpha\beta}(k)$, and the modified structure of the nonlinear spectral transfer term $h^{NL}_{\alpha\beta}(k)$. The fact that the coherency spectrum initially decreases suggests that mean gradient effects

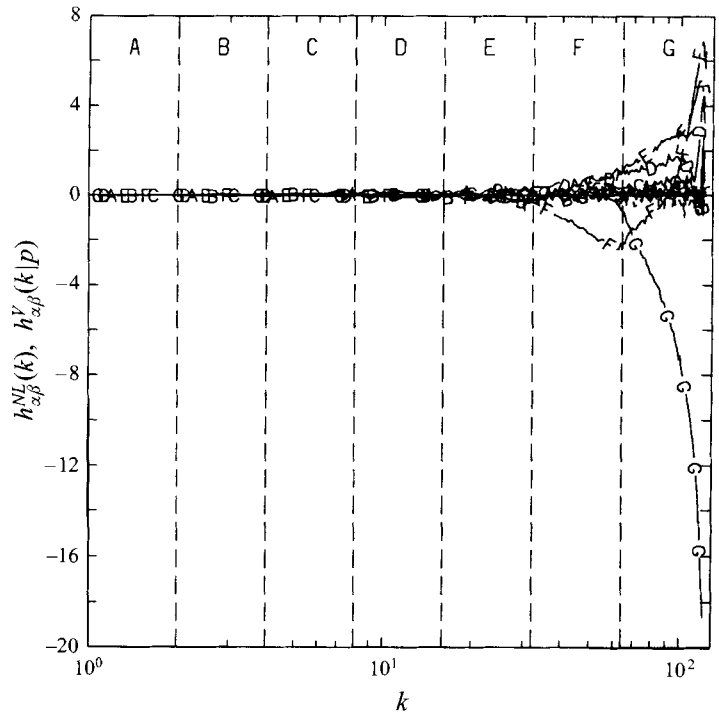

FIGURE 23. Decomposition of the spectral transfer contributions $h^{NL}_{\alpha\beta}(k)$ (dashed line) to the coherency evolution spectrum into contributions $h^{V}_{\alpha\beta}(k|p)$ from velocity modes in logarithmically spaced ranges A–G, for a pair of scalars with $Sc = 1/8$ and 1 in the stationarity period (averaged from $t/T_E = 1.921$ to 18.57) in differential diffusion with uniform mean gradients in a 256^3 simulation at $R_\lambda = 160$.

are initially weak, although their importance grows in time. Physically, mean gradient effects are associated with the large scales in the velocity field (which account for most of the production of scalar fluctuations), whereas de-correlation at high wavenumbers is primarily caused by (as seen in §4.2) the action of small scales in the velocity field. Consequently, at early times the latter effect having a shorter characteristic time is felt sooner than the mean gradient effects which have longer time scales.

Figure 22 shows the relative roles of $h^{NL}_{\alpha\beta}(k)$ and $m_{\alpha\beta}(k)$, at early times corresponding to lines A and B in figure 20, and at later times by time averaging. Because of limited resolution, the behaviour at the highest wavenumbers $k > 110$ is best regarded as numerically spurious. At the earliest time shown ($0.128T_E$, or 2.4 τ_η), the mean gradient contribution is seen to be coherent, but much weaker than the overall de-correlating effect of nonlinear triadic interactions. Over time, the mean gradient contribution remains coherent, with magnitude first increasing and then decreasing in time. Despite substantial statistical jitter, the spectral transfer term is seen to be de-correlating at high wavenumbers. The relative strength of this de-correlation is especially strong at early times, but decreases steadily with time. At later times we find, consistent with the attainment of statistical stationarity in the coherency spectrum, an approximate balance at the small scales between coherent mean gradient production and incoherent spectral transfer contributions.

The manner in which the spectral transfer contributions to the evolution of coherency are modified by uniform mean gradients is of great interest, especially in

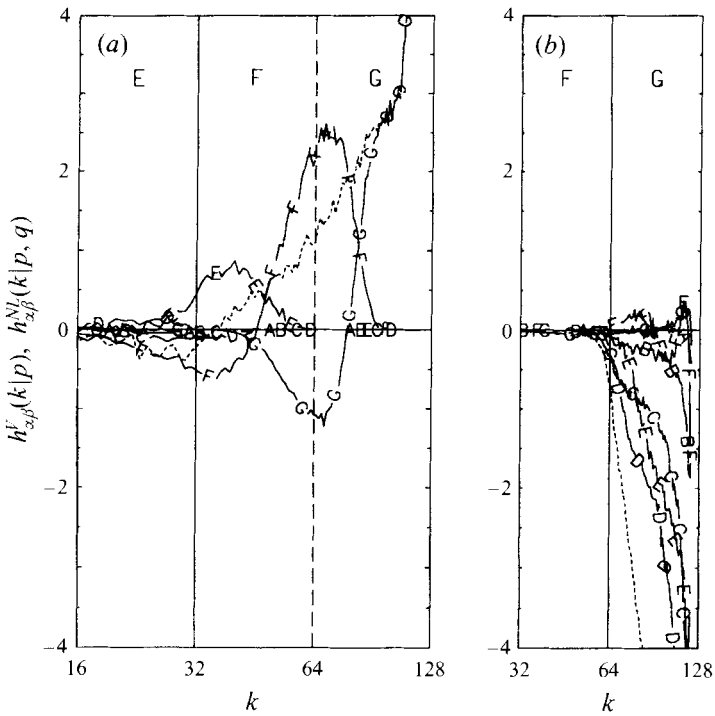

FIGURE 24. Decomposition of the velocity-mode contribution $h^V_{\alpha\beta}(k|p)$ (dashed line) to the coherency evolution spectrum for selected ranges of p in the data of figure 23: (*a*) $16 \leqslant p < 32$ (range E), (*b*) $64 \leqslant p < 128$ (range G), into detailed contributions $h^{NL}_{\alpha\beta}(k|p,q)$ from scalar modes q in the logarithmically spaced ranges A–G. The data are essentially zero at wavenumbers lower than the range shown.

the later time period when stationarity is attained. Figure 23 shows the transfer contributions $h^V_{\alpha\beta}(k|p)$ from velocity modes for a pair of scalars at $Sc = 1/8$ and 1 in the stationary state. At high wavenumbers, the total transfer term $h^{NL}_{\alpha\beta}(k)$ (dashed line, partly hidden) is seen to be the net result of strong mutual cancellation between negative (de-correlating) contributions from velocity modes in the highest octave and positive (coherent) contributions from the rest of velocity modes at lower wavenumber. Contributions from lower-wavenumber velocity modes p (up to range E) are essentially entirely coherent for all wavenumbers k, increasing in magnitude with k. Velocity modes p in the highest octave (range G) have no significant effect on scalar modes of lower wavenumber (for k in range F or lower, when the velocity mode is likely to be the longest leg in the triads), but have a de-correlating effect on high-wavenumber scalar modes that increases in magnitude rapidly with wavenumber. Velocity modes in range F display intermediate behaviour: they are de-correlating when the scale ratio between p and k is about 3 or less, but correlating as the scale ratio increases further with wavenumber. The strongest coherent contributions come from only moderately non-local (p in ranges E and F) rather than highly non-local interactions (p in ranges A to C). These observations are qualitatively consistent with the analysis presented in §4.2 for the case of no mean scalar gradients. However, the presence of mean gradients appears to enhance the relative strength of the coherent contributions from velocity modes of wavenumber lower than the scalar modes.

More detailed information on transfer contributions from the most strongly corre-

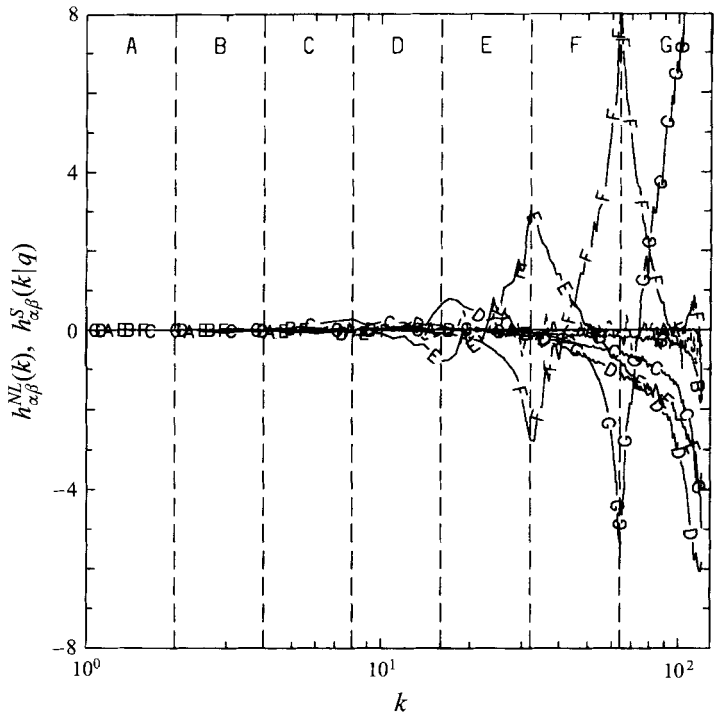

FIGURE 25. Decomposition of the spectral transfer contributions $h^{NL}_{\alpha\beta}(k)$ (dashed line) to the coherency evolution spectrum into contributions $h^{S}_{\alpha\beta}(k|q)$ from scalar modes q in the logarithmic ranges A–G (for the data of figure 23).

lating (range E) and most strongly decorrelating (range G) octave of velocity modes is given in figure 24(a,b) via the functions $h^{NL}_{\alpha\beta}(k|p,q)$ for different ranges of the other scalar mode q in the triads. It is clearly seen in figure 24(a) that the effect of the correlating triads is a forward cascade, which tends to decrease coherency at lower wavenumbers but increase coherency at higher wavenumbers. For example, the negative loop in line F ($32 \leqslant p < 64$) represents the effect on scalars at wavenumber k when $p < k < q$, whereas the positive loop indicates the effect on k for $p < q < k$. Furthermore, as seen earlier in this paper, the forward cascade is relatively local between the scalar modes.

It may be seen in figure 24(b) that de-correlating effects at high wavenumbers k are primarily caused by triads in which $q < p < k$, with the velocity mode being intermediate in scale. The strongest contributions for k in range G are associated with the other scalar mode q in range D, indicating that the de-correlating triads are moderately, but not strongly, non-local between the scalar modes q and k.

Figure 25 shows the transfer contributions $h^{S}_{\alpha\beta}(k|q)$ for different ranges of scalar modes q. The presence of a coherent local forward cascade between scalar modes is clearly seen (lines E, F and G). Whereas some evidence of a similar cascade may be found in later-time results without mean gradients (figure 19), when mean gradients are present the observed forward cascade behaviour is much more pronounced and well-maintained. The localness of this cascade is also well demonstrated: for example, at sufficiently high wavenumbers when the scale disparity between the scalar modes q and k is greater than about 4, line E ceases to be positive (in fact, becoming strongly

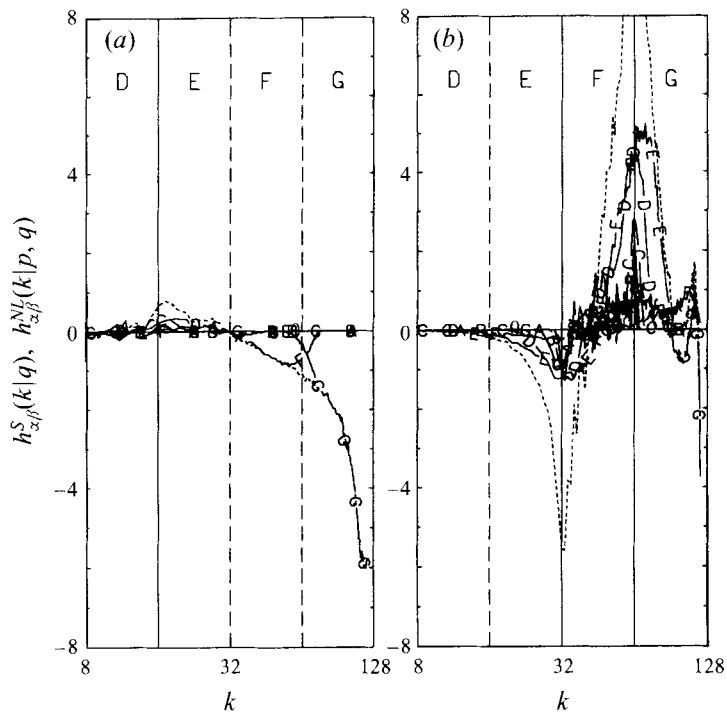

FIGURE 26. Decomposition of the scalar-mode contribution $h^S_{\alpha\beta}(k|q)$ (dashed line) to the coherency evolution spectrum for selected ranges of q in the data of figure 23: (*a*) $8 \leqslant q < 16$ (range D), (*b*) $32 \leqslant q < 64$ (range F), into detailed contributions $h^{NL}_{\alpha\beta}(k|p,q)$ from velocity modes p in the logarithmically spaced ranges A–G. The data are essentially zero at wavenumbers lower than the range shown.

de-correlating). Negative values of $h^S_{\alpha\beta}(k|q)$ at high wavenumbers associated with q in the range D correspond to the de-correlating triads shown in figure 24(*b*).

Detailed triadic contributions to $h^S_{\alpha\beta}(k|q)$ for q in the most actively de-correlating and correlating ranges (D and F respectively) are shown in figure 26(*a*, *b*). The former indicates that the de-correlating triads are formed from non-local interactions between scalar modes of disparate scales (with a ratio of 8 between ranges D and G) coupled to a high-wavenumber velocity mode. At the same time, figure 26(*b*) confirms that the coherent forward cascade is caused by local interactions between scalar modes of similar size (ranges F and G) coupled by a relatively low-wavenumber velocity mode (ranges D and E).

In addition to understanding the nature of spectral transfer in the stationary state (as above), we are interested in obtaining an estimate of the time it takes for the mean gradient modifications of multi-scalar spectral transfer to become significant. This requires examination of early-time results, which in turn requires ensemble averaging over multiple realizations, since time averaging is no longer applicable. To limit computational expense, we consider early-time results from 128^3 simulations at $R_\lambda = 90$, with 17 realizations. The breakdowns of transfer contributions $h^V_{\alpha\beta}(k|p)$ (for velocity modes) and $h^S_{\alpha\beta}(k|q)$ (for scalar modes) are shown in figures 27 and 28 respectively, at 0.9 eddy-turnover times for two scalars at $Sc = 1/8$ and 1. It is clear that both correlating and de-correlating effects have the same trends as in the stationary-state results of figures 23 and 25. The differences are a matter of degree,

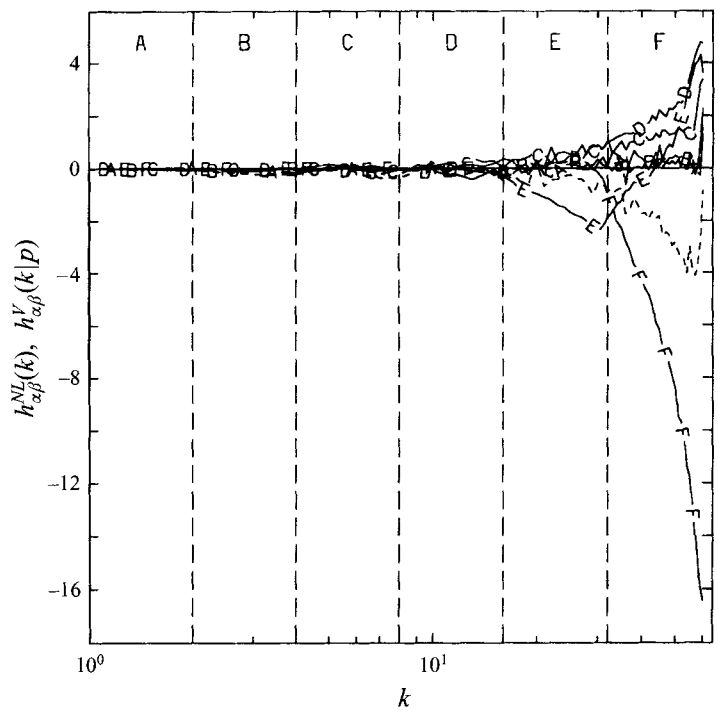

FIGURE 27. Decomposition of the spectral transfer contributions $h^{NL}_{\alpha\beta}(k)$ (dashed line) to the coherency evolution spectrum into contributions $h^{V}_{\alpha\beta}(k|p)$ from velocity modes in logarithmically spaced ranges A–F, for a pair of scalars with $Sc = 1/8$ and 1 at an early-time $(t/T_E = 0.9)$ in differential diffusion with uniform mean gradients in a 128^3 simulation at $R_\lambda = 90$.

in that at early times coherent forward cascade effects are not yet as strong as the de-correlating effects of high-wavenumber velocity modes, so that the overall transfer contribution is negative at high wavenumbers. It is found that the negative transfer $h^{NL}_{\alpha\beta}(k)$ in this particular dataset is nearly balanced by a coherent mean gradient contribution $m_{\alpha\beta}(k)$. Together with the results of figure 20, these observations indicate that the characteristic time for mean gradient effects to be felt strongly is on the order of the eddy-turnover time, which is a time scale of the large-scale motions. This is perhaps not surprising, since mean gradient effects are a result of velocity fluctuations (with the eddy-turnover time as characteristic time scale) acting on the uniform mean scalar gradients.

Because the presence of uniform mean scalar gradients constitutes a source of scalar fluctuations with the same spectral form as the velocity fluctuations, it may be expected that some aspects of differential diffusion viewed in Fourier space would be sensitive to scale differences between velocity and scalar fields. In particular, for a low-Schmidt-number scalar the spectral peak of the source will be located at a wavenumber higher than that of the scalar fluctuations. Whereas all later-time spectral transfer characteristics are similar for all three pairs of scalars in the simulations, we find that at early times the pair with $Sc = 1/8$ and $1/4$ (both significantly less than unity) behave differently. For this pair of scalars, at the time $(t/T_E = 0.9)$ of the results of figures 27 and 28 it is found that at high wavenumbers $m_{\alpha\beta}(k)$ is negative, whereas $h^{NL}_{\alpha\beta}(k)$ is positive.

Whereas the de-correlating nature of mean gradients at early times for highly

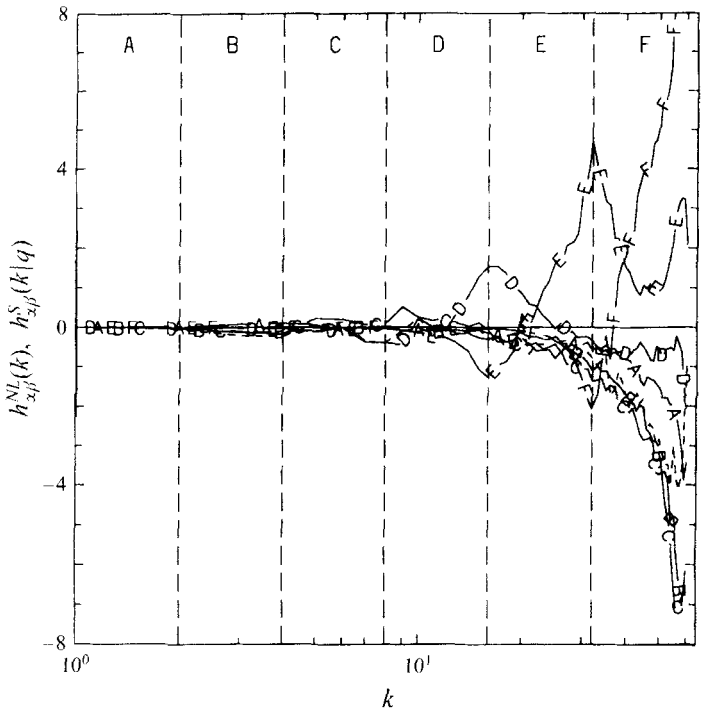

FIGURE 28. Decomposition of the spectral transfer contributions $h^{NL}_{\alpha\beta}(k)$ (dashed line) to the coherency evolution spectrum into contributions $h^S_{\alpha\beta}(k|q)$ from scalar modes q in the logarithmic ranges A–F (for the data of figure 27).

diffusive scalars may seem somewhat surprising, it can be traced to differences in spectral shape. Consider, for simplicity, the case in which $\nabla\Phi_\alpha = \nabla\Phi_\beta$, and let ϕ_α be the more diffusive scalar with lower Schmidt number. The mean gradient effect $m_{\alpha\beta}(k)$ as given in (14) consists of four terms in its numerator, listed here in the order (I) $e_{\alpha\alpha}e_{\alpha\beta}f_{i\beta}$, (II) $-e_{\alpha\alpha}e_{\beta\beta}f_{i\alpha}$, (III) $e_{\alpha\beta}e_{\beta\beta}f_{i\alpha}$, (IV) $-e_{\alpha\alpha}e_{\beta\beta}f_{i\beta}$. When the mean gradients are positive the scalar flux contributions $f_{i\alpha}$ and $f_{i\beta}$ are negative on average. Because $Sc_\beta > Sc_\alpha$, and especially if they differ greatly, at high wavenumbers one expects $|f_{i\beta}| > |f_{i\alpha}|$ and (of course) $e_{\beta\beta} > e_{\alpha\alpha}$ on average. Furthermore, the ratio between the spectra of different scalars is found to be greater than the ratio between their corresponding flux spectra. Consequently, in general, terms III (>I) and IV (<II) provide the strongest positive and negative contributions respectively. For scalars with Sc 1/8 and 1/4 it is found that the spectral shapes are such that the overall mean gradient effect $m_{\alpha\beta}(k)$ is nearly zero at most wavenumbers, and slightly negative at the highest few wavenumber shells. For the other two pairs (1/8 and 1; 1/4 and 1) the mean gradient contribution is definitely positive, although dropping off in magnitude at the highest-wavenumber shells.

5. Conclusions

Detailed analyses of spectral transfer by triadic interactions have been performed on direct numerical simulation data to investigate the spectral mechanisms of the differential diffusion of multiple scalars. Simulations using a massively parallel computer code have been carried out for scalars with Schmidt numbers (Sc) from

1/8 to 1 in forced stationary isotropic turbulence, with Taylor-scale Reynolds number $R_\lambda = 90$ on an 128^3 grid without mean scalar gradients, and $R_\lambda = 160$ on a 256^3 grid with uniform mean scalar gradients. The $R_\lambda = 160$ velocity fields possess a short inertial range in the energy spectrum, and contain a range of scales comparable to that found in an axisymmetric jet of mean flow Reynolds number about 34 000 based on the exit diameter. Appropriate evolution equations have been derived in order to understand the roles of different processes in the development of the spectral coherency between different scalars, which measures their phase alignment in Fourier space.

The conclusions of this work are summarized below, corresponding to the questions raised at the beginning of §4.

First, a recent study of single-scalar spectral transfer (Yeung 1994) has been extended to higher Reynolds number, a wide range of Schmidt numbers, and scalar fields generated by velocity fluctuations acting upon uniform mean scalar gradients. All results indicate, as before, a robust local forward cascade behaviour in which scalar fluctuations are generated at successively smaller scales. The wider range of scales present at higher Reynolds number allows us to distinguish between the effects of triads of varying degrees of locality–non-locality. The transfer is found to be moderately non-local between a scalar mode at wavenumber k and the velocity mode p that provides the coupling between two scalar modes in a triad in wavenumber space. This conclusion is supported by an analysis based on the scale disparity parameter proposed by Zhou (1993*a*, *b*) for energy transfer. It is suggested that the velocity scales contributing most to the forward cascade are located near the peak of the dissipation spectrum. This physical picture is not greatly altered by low Schmidt number or uniform mean gradients. However in these cases there is more transfer activity at lower wavenumbers, primarily because the scalar spectrum is more concentrated at the lower wavenumbers, due to higher molecular diffusivity or mean gradient production at the large scales.

Second, the rapid de-correlation observed at the small scales in differential diffusion at early times is found to be primarily a result of the action of small scales in the velocity field – which, however, contribute little to the spectral transfer of each scalar. For high-wavenumber scalar modes k, the most strongly de-correlating triads are of the type $q < p < k$, in which the scalar mode k is coupled to another mode q via a velocity mode p that is intermediate in scale, and especially so when the scale separation between k and q is moderately non-local (around $k/q \approx 4$ at 0.5 Kolmogorov time scales in the simulations at $R_\lambda = 90$). These de-correlating triads are counteracted by a coherent local forward cascade represented by triads of the type $p < q < k$, in which q is close in magnitude to k, and the separation between p and k is (consistent with single-scalar results) moderately non-local. This spectral flux carries relatively coherent scalar fluctuations towards higher wavenumbers, and is particularly effective when the coherency spectrum decreases steeply with wavenumber. However, at early times in differential diffusion this coherent cascade effect is weaker than the de-correlating effect of triads of the type $q < p < k$. This scenario of fundamentally different types of different triadic interactions being responsible for the spectral cascade of the scalars and the spectral propagation of differential diffusion is consistent with the work of Kerstein, Cremer & McMurtry (1995).

Third, in the absence of mean scalar gradients, despite considerable statistical variability, we find that the slow rate of change of coherency at later times is caused by an approximate balance between triads of the type $q < p < k$ (which continue to be strongly de-correlating) and those of the type $p < q < k$ (whose coherent cascade

effect grows in relative strength with time). With a coherency spectrum that now exhibits a definite negative slope across a wide range of scales, both opposing effects above are felt at intermediate as well as high wavenumbers. The de-correlating triadic interactions become more non-local, because a wider scale separation between modes k and q is now required for them to exhibit a significant difference in coherency.

Finally, production by uniform mean gradients (primarily at the large scales) alters coherency development both directly through an explicit contribution to the coherency evolution equation and indirectly via influencing the spectral transfer contributions. A statistically stationary state is observed for the coherency spectrum, as a result of a balance between a coherent mean gradient production term and a spectral transfer term that is de-correlating overall, albeit of relatively small magnitude. The maintenance of high coherency at the large scales by mean gradients in the stationary state is consistent with the mixing-layer measurements of Li *et al.* (1993), which showed that, especially near the centreline, the scalars remain highly coherent in the frequency domain except at very high frequencies. The coherent local forward cascade effect is well maintained by the mean gradients, and much more pronounced than that in the case of no mean scalar gradients. Strong mutual cancellation is observed between correlating and de-correlating triads. Such triads are still of the types $p < q < k$ and $q < p < k$ respectively, and characterized by a moderate degree of non-localness. Mean gradient effects are strongly felt within a characteristic time of about 1 eddy-turnover time. Transient effects that can be traced to differences in spectral shape are observed for scalar pairs of low Schmidt number.

In summary, this paper provides a quantitative description of the spectral mechanisms of differential diffusion in turbulent flow, in which the relative spectral content and scale separation among velocity and multiple scalar fields play a crucial role. Production by uniform mean gradients can be viewed as just one (but important) example of a source of scalar fluctuations, with the same spectral content as the velocity fields. Many interesting questions remain in the general case in which scalar fluctuations may be added or removed at different scales. The effects of such scale-dependent production or destruction terms due to chemical processes would be of special interest in the study of differential diffusion of reacting scalars, which is itself a problem of great practical significance in turbulent combustion. The physical understanding achieved for passive, inert scalars in this work is expected to be important for future efforts directed at the more general reacting case.

The author gratefully acknowledges support from the National Science Foundation, through Grants CTS-930793 and CTS-9411690. He also thanks Professor James G. Brasseur as well as Drs Jeffrey R. Chasnov, Alain Pumir, and Chenning Tong for valuable discussions on aspects of this work. Mr B. Luo and Ms C.A. Moseley assisted in performing some of the numerical simulations.

This research was conducted in part using the supercomputing resources of the Cornell Theory Center, which receives major funding from the National Science Foundation and New York State. Additional funding comes from the Advanced Research Projects Agency, the National Institutes of Health, IBM Corporation and other members of the center's Corporate Research Institute.

Appendix. Computation of coherency from DNS data

In direct numerical simulations of isotropic turbulence with a discrete set of Fourier modes, it is customary to collect numerically computed spectra into spherical

wavenumber shells of finite thickness Δk (usually taken as unity for convenience). We demonstrate in this Appendix that the precise manner in which this practice is carried out can have non-trivial effects on the representation of the spectral coherency between multiple scalars.

The definition adopted for the spectral coherency in this paper is given by (9), which may also be as written as

$$\rho_{\alpha\beta}(k) = \left\langle \frac{1}{N(k)} \sum_{\Delta k} \frac{e_{\alpha\beta}(\boldsymbol{k}')}{[e_{\alpha\alpha}(\boldsymbol{k}')e_{\beta\beta}(\boldsymbol{k}')]^{1/2}} \right\rangle , \tag{A 1}$$

where within each realization the coherency is a measure of the average degree of alignment between the different scalars among Fourier modes in a given wavenumber shell. On the other hand, if we define the coherency via the usual spectra and co-spectra (which are pre-collected into the wavenumber shells, as $E^{\phi}_{\alpha\beta}(k) = \sum_{\Delta k} \langle e_{\alpha\beta}(\boldsymbol{k}') \rangle$, etc.), we obtain the quantity

$$\rho^{*}_{\alpha\beta}(k) = \frac{E^{\phi}_{\alpha\beta}(k)}{[E^{\phi}_{\alpha\alpha}(k)E^{\phi}_{\beta\beta}(k)]^{1/2}} , \tag{A 2}$$

which was used previously in Yeung & Pope (1993) and Yeung & Moseley (1995a).

The two definitions above, which we characterize as 'modal' and 'shellwise' respectively, are not equivalent. In particular, whereas two Fourier modes within a given shell with the same phase difference between the scalars $\hat{\phi}_{\alpha}(\boldsymbol{k}')$ and $\hat{\phi}_{\beta}(\boldsymbol{k}')$ contribute equally to $\rho_{\alpha\beta}(k)$, their contributions to the numerator of $\rho^{*}_{\alpha\beta}(k)$ will be weighted by the magnitude of their relative spectral content. Except perhaps in the lowest couple of wavenumber shells, the decrease of the spectra and co-spectra with wavenumber implies that within a given shell, modes of lower k' will contribute more heavily since they have more spectral content than modes of slightly higher k' in the same shell. Furthermore, because in general scalar fluctuations at larger scales are less strongly affected by differential diffusion (i.e. are less strongly de-correlated), the contributions from these modes of lower k' are likely to be more coherent. Consequently, whereas the two definitions may give qualitatively similar results, one may expect $\rho^{*}_{\alpha\beta}(k)$ to be higher than $\rho_{\alpha\beta}(k)$ in most situations, especially when the coherency spectrum decreases steeply with wavenumber. On the other hand, if the coherency spectrum is relatively flat the difference in coherency between modes in a given shell would be less significant, so that the difference between $\rho_{\alpha\beta}(k)$ and $\rho^{*}_{\alpha\beta}(k)$ should be much less.

To illustrate these arguments it is sufficient to compare results from a single 64^3 realization without mean gradients. Figure 29 shows, using different symbols, the quantities $\rho_{\alpha\beta}(k)$ and $\rho^{*}_{\alpha\beta}(k)$ at an early time when the coherency spectrum is relatively steep, and at a later time when the coherency spectrum is relatively flat. It is clearly seen, as argued above, that in general $\rho^{*}_{\alpha\beta}(k)$ is higher than $\rho_{\alpha\beta}(k)$, especially at high wavenumbers in the early time period when coherency decreases steeply. Also shown for comparison is the quantity $\hat{\rho}_{\alpha\beta}(k)$, which is a degenerate form of $\rho_{\alpha\beta}(k)$ in which only modes of wavenumber magnitude exactly equal to k are considered (in effect, with $\Delta k = 0$). In this way, $\hat{\rho}_{\alpha\beta}(k)$ provides, in principle, an estimation of coherency without the numerical artifact of finite-thickness wavenumber shells. However, since in the simulations the number of such Fourier modes of the same wavenumber magnitude is small, the computed $\hat{\rho}_{\alpha\beta}(k)$ is, as may be seen, very noisy. A reasonable smoothing is provided by $\rho_{\alpha\beta}(k)$, through the process of averaging over modes of approximately the same scale size within the spectral shell. Consequently,

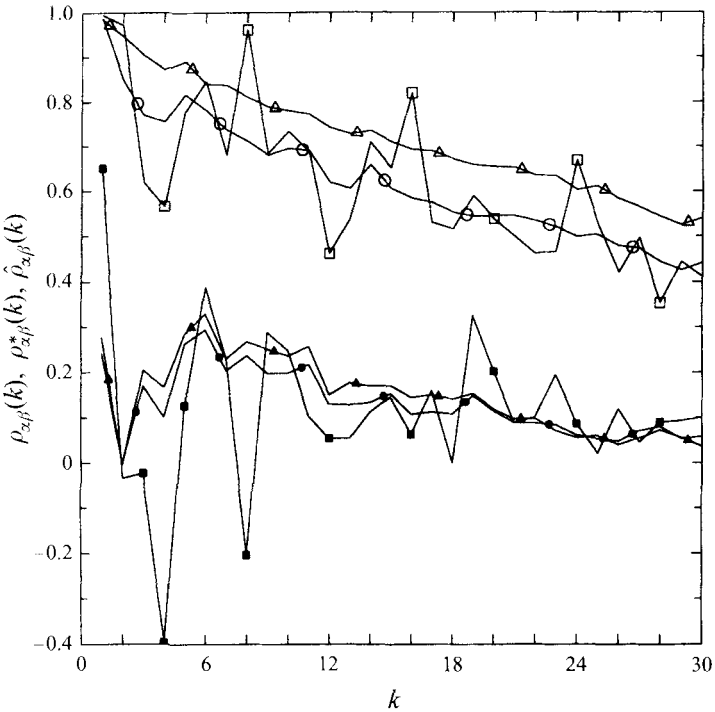

FIGURE 29. Comparison of three definitions of coherency spectrum computed from DNS data: $\rho_{\alpha\beta}(k)$ (triangles), $\rho^*_{\alpha\beta}(k)$ (circles), and $\hat{\rho}_{\alpha\beta}(k)$ (squares) in a 64^3 simulation: at an early time $t/T_E = 2.5$ when $\rho_{\alpha\beta} = 0.867$ (open symbols) and a later time $t/T_E = 25$ when $\rho_{\alpha\beta} = 0.182$ (closed symbols).

of the three quantities shown, the modal definition $\rho_{\alpha\beta}(k)$ appears to provide the best representation of coherency as a function of scale, and is therefore adopted in this paper.

The later-time data shown in figure 29 also support the argument that when the coherency spectrum is relatively flat (which occurs at large times in the absence of mean gradients), the difference between $\rho_{\alpha\beta}(k)$ and $\rho^*_{\alpha\beta}(k)$ should be relatively small. Increased statistical variability at later times is also evident, especially for $\hat{\rho}_{\alpha\beta}(k)$ at low wavenumbers.

Besides taking on different numerical values, the quantities $\rho_{\alpha\beta}(k)$ and $\rho^*_{\alpha\beta}(k)$ do not satisfy the same evolution equation. The evolution of $\rho_{\alpha\beta}(k)$ is given by (12)–(15), which are based on averaging the rates of change of coherency over the modes within each wavenumber shell. In particular, coherency evolution at a single Fourier mode is given by (13), which is characterized by the absence of molecular diffusivities. However, this equation does not readily generalize to the shellwise coherency $\rho^*_{\alpha\beta}(k)$, because – as may be shown by straightforward algebra – complete cancellation of molecular terms in $\partial\rho^*_{\alpha\beta}(k)/\partial t$ would require the quantity

$$-\sum_{\Delta k} e_{\alpha\alpha} \sum_{\Delta k} e_{\beta\beta} \sum_{\Delta k} (D_\alpha + D_\beta) k^2 e_{\alpha\beta} + \sum_{\Delta k} e_{\alpha\beta} \sum_{\Delta k} e_{\alpha\alpha} \sum_{\Delta k} D_\beta k^2 e_{\beta\beta} + \sum_{\Delta k} e_{\alpha\beta} \sum_{\Delta k} e_{\beta\beta} \sum_{\Delta k} D_\alpha k^2 e_{\alpha\alpha}$$

to vanish. For any finite shell thickness Δk a complete cancellation is not possible, because the wavenumber magnitude k varies within each shell, so that, for

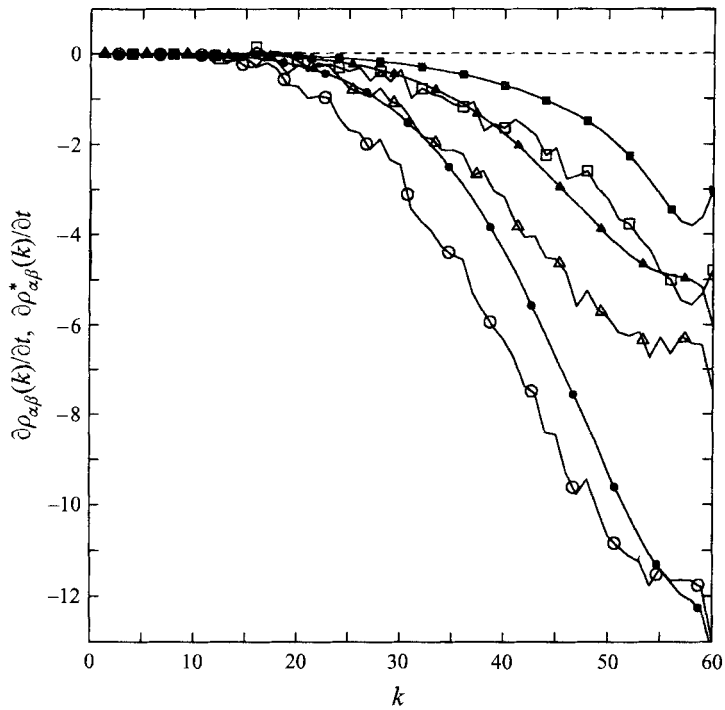

FIGURE 30. Comparison of coherency evolution spectra according to the modal (open symbols) and shellwise (closed symbols) definitions, for three pairs of scalars at $Sc = 1/8$ and $1/4$ (triangles); $1/8$ and 1 (circles); and $1/4$ and 1 (squares), from ensemble-averaged early-time results in 128^3 simulations.

example,

$$\sum_{\Delta k} e_{\beta\beta} \sum_{\Delta k} k^2 e_{\alpha\beta} \neq \sum_{\Delta k} e_{\alpha\beta} \sum_{\Delta k} k^2 e_{\beta\beta} \,.$$

In other words, the exact expression for $\partial\rho^*_{\alpha\beta}(k)/\partial t$ (in the absence of mean gradients) contains some residual molecular diffusivity effects arising from the use of a finite (arbitrary) shell thickness in collecting the spectra. This limitation provides additional justification for adopting the 'modal' definition $\rho_{\alpha\beta}(k)$ instead.

On the other hand, numerical tests suggest that the discrepancy due to imperfect cancellation of molecular terms in $\partial\rho^*_{\alpha\beta}(k)/\partial t$ is small in practice, except at low wavenumbers where the shell thickness (Δk) is a significant fraction of the shell radius (k). At early times, the coherency evolution rate at low wavenumbers is itself expected to be small. Consequently, a good (albeit inexact) approximation of the nonlinear part of $\partial\rho^*_{\alpha\beta}(k)/\partial t$ is still given by

$$\left.\frac{\partial\rho^*_{\alpha\beta}(k)}{\partial t}\right|_{\mathrm{NL}} \approx \left[E^\phi_{\alpha\alpha}E^\phi_{\beta\beta}\right]^{-3/2}\left[E^\phi_{\alpha\alpha}E^\phi_{\beta\beta}T_{\alpha\beta} - \tfrac{1}{2}E^\phi_{\alpha\alpha}E^\phi_{\alpha\beta}T_{\beta\beta} - \tfrac{1}{2}E^\phi_{\beta\beta}E^\phi_{\alpha\beta}T^\phi_{\alpha\alpha}\right]$$

(where the upper-case symbols represent sums over spectral shells).

The evolution rates of $\rho_{\alpha\beta}(k)$ and $\rho^*_{\alpha\beta}(k)$ are compared in figure 30 for 128^3 simulations at early times and without mean scalar gradients. The data shown for (the nonlinear part of) $\partial\rho_{\alpha\beta}(k)/\partial t$ are the same as in figure 13. It is seen that the shellwise coherency decreases more slowly, consistent with the observation of $\rho_{\alpha\beta}(k) > \rho^*_{\alpha\beta}(k)$ in the early-time results in figure 29. The shellwise data are also

much smoother, which indicates that some statistical variability is removed when the spectra and co-spectra are summed over the Fourier modes in each shell.

REFERENCES

BATCHELOR, G. K. 1959 Small-scale variation of convected quantities like temperature in turbulent fluid. Part 1. General discussion and the case of small conductivity. *J. Fluid Mech.* **5**, 113–133.

BILGER, R. W. & DIBBLE, R. W. 1982 Differential molecular diffusion effects in turbulent mixing. *Combust. Sci. Tech.* **28**, 161–172.

BRASSEUR, J. G. & WEI, C.-H. 1994 Interscale dynamics and local isotropy in high Reynolds number turbulence within triadic interactions. *Phys. Fluids* **6**, 842–870.

CHASNOV, J. R. 1994 Similarity states of passive scalar transport in isotropic turbulence. *Phys. Fluids* **6**, 1036–1051.

CORRSIN, S. 1951 On the spectrum of isotropic temperature fluctuations in an isotropic turbulence. *J. Appl. Phys.* **22**, 469–473.

DOMARADZKI, J. A. & ROGALLO, R. S. 1990 Local energy transfer and nonlocal interactions in homogeneous, isotropic turbulence. *Phys. Fluids* A **2**, 413–426.

ESWARAN, V. & POPE, S. B. 1988*a* An examination of forcing in direct numerical simulations of turbulence. *Comput. & Fluids* **16**, 257–278.

ESWARAN, V. & POPE, S. B. 1988*b* Direct numerical simulations of the turbulent mixing of a passive scalar. *Phys. Fluids* **31**, 506–520.

JABERI, F. A., MILLER, R. S., MADNIA, C. K. & GIVI, P. 1995 Non-Gaussian scalar statistics in homogeneous turbulence. *Proc. Tenth Symp. on Turbulent Shear Flows*, pp. 31-13–31-18. University Park, PA.

JAYESH & WARHAFT, Z. 1992 Probability distribution, conditional dissipation, and transport of passive temperature fluctuations in grid-generated turbulence. *Phys. Fluids* A **4**, 2292–2307.

JIMENEZ, J., WRAY, A. A., SAFFMAN, P. G. & ROGALLO, R. S. 1993 The structure of intense vorticity in isotropic turbulence. *J. Fluid Mech.* **255**, 65–90.

KERSTEIN, A. R., CREMER, M. A. & MCMURTRY, P. A. 1995 Scaling properties of differential molecular diffusion effects in turbulence. *Phys. Fluids* **7**, 1999–2007.

KOLMOGOROV, A. N. 1941 The local structure of turbulence in incompressible viscous fluids for very large Reynolds numbers. *C. R. Acad. Sci. URSS* **30**, 301–305.

KOMORI, S., HUNT, J. C. R., KANZAKI, K. & MURAKAMI, Y. 1991 The effects of turbulent mixing on the correlation between two species and on concentration fluctuations in non-premixed reacting flows. *J. Fluid Mech.* **228**, 629–659.

KOSÁLY, G. 1993 Frequency spectra of reactant fluctuations in turbulent flows. *J. Fluid Mech.* **246**, 489–502.

LI, J. D., BROWN, R. J. & BILGER, R. W. 1993 Spectral measurement of reactive and passive scalars in a turbulent reactive-scalar mixing layer. *Proc. Ninth Symp. on Turbulent Shear Flows*, paper 28-3. Kyoto, Japan.

NILSEN, V. & KOSÁLY, G. 1996 Differentially diffusing scalars in turbulence. Submitted to *Phys. Fluids*.

OBUKHOV, A. M. 1949 Structure of the temperature field in a turbulent flow. *Izv. Akad. Nauk SSSR Geogr. Geofiz.* **13**, 58–69.

POPE, S. B. 1990 Computations of turbulent combustion: progress and challenges. *Twenty-Third Symposium (International) on Combustion*, pp. 591–612. The Combustion Institute (invited plenary lecture).

PUMIR, A. 1994 A numerical study of the mixing of a passive scalar in three-dimensions in the presence of a mean gradient. *Phys. Fluids* **6**, 2118–2132.

ROGALLO, R. S. 1981 Numerical experiments in homogeneous turbulence. *Tech. Memo.* 81315. NASA Ames Research Center.

ROGERS, M. M., MOIN, P. & REYNOLDS, W. C. 1986 The structure and modeling of the hydrodynamic and passive scalar fields in homogeneous turbulent shear flow. *Rep.* TF-25. Dept of Mech. Engng, Stanford University.

SAYLOR, J. R. & SREENIVASAN, K. R. 1993 Differential diffusion in low Reynolds number water jets. *J. Fluid Mech.* (submitted).

SIRIVAT, A. & WARHAFT 1982 The mixing of passive helium and temperature fluctuations in grid turbulence. *J. Fluid Mech.* **120**, 475–504.

SMITH, L. L. 1994 Differential molecular diffusion in reacting and non-reacting turbulent jets of H_2CO_2 mixing with air. PhD dissertation, Department of Mechanical Engineering, University of California at Berkeley.

SREENIVASAN, K. R. 1991 On the local isotropy of passive scalars in turbulent shear flows. In *Turbulence and Stochastic Processes: Kolmogorov's ideas 50 years on* (ed. J. C. R. Hunt, O. M. Phillips & D. Williams), pp. 165–182. Royal Society, London.

TONG, C. & WARHAFT, Z. 1995 Passive scalar dispersion and mixing in a turbulent jet. *J. Fluid Mech.* **292**, 1–38.

VINCENT, A. & MENEGUZZI, M. 1991 The spatial structure and statistical properties of homogeneous turbulence. *J. Fluid Mech.* **225**, 1–20.

WANG, L. P., CHEN, S., BRASSEUR, J. G. & WYNGAARD, J. C. 1996 Examination of fundamental hypotheses in the Kolmogorov refined turbulence theory through high-resolution simulation. *J. Fluid Mech.* **309**, 113–156.

WARHAFT, Z. & LUMLEY, J. L. 1978 An experimental study of the decay of temperature fluctuations in grid-generated turbulence. *J. Fluid Mech.* **88**, 659–684.

YEH, T. T. & VAN ATTA, C. W. 1973 Spectral transfer of scalar and velocity fields in heated-grid turbulence. *J. Fluid Mech.* **58**, 233–261.

YEUNG, P. K. 1994 Spectral transfer of self-similar passive scalar fields in isotropic turbulence. *Phys. Fluids* **6**, 2245–2247.

YEUNG, P. K. & BRASSEUR, J. G. 1991 The response of isotropic turbulence to isotropic and anisotropic forcing at the large scales. *Phys. Fluids* A **3**, 884–897.

YEUNG, P. K., BRASSEUR, J. G. & WANG, Q. 1995 Dynamics of large-to-small scale couplings in coherently forced turbulence: concurrent physical and Fourier space views. *J. Fluid Mech.* **283**, 43–95.

YEUNG, P. K. & LUO, B. 1995 Simulation and modeling of differential diffusion in homogeneous turbulence. *Proc. Tenth Symp. on Turbulent Shear Flows*, pp. 31–7–31–12. University Park, PA.

YEUNG, P. K. & MOSELEY, C. A. 1995*a* Effects of mean scalar gradients on differential diffusion in isotropic turbulence. *AIAA Paper* 95-0866.

YEUNG, P. K. & MOSELEY, C. A. 1995*b* A message-passing, distributed memory parallel algorithm for direct numerical simulation of turbulence with particle tracking. In *Parallel Computational Fluid Dynamics: Implementations and Results Using Parallel Computers* (ed. A. Ecer, J. Periaux, N. Satofuka & S. Taylor). Elsevier.

YEUNG, P. K. & POPE, S. B. 1989 Lagrangian statistics from direct numerical simulations of isotropic turbulence. *J. Fluid Mech.* **207**, 531–586.

YEUNG, P. K. & POPE, S. B. 1993 Differential diffusion of passive scalars in isotropic turbulence. *Phys. Fluids* A **5**, 2467–2478.

ZHOU, Y. 1993*a* Degrees of locality of energy transfer in the inertial range. *Phys. Fluids* A **5**, 1092–1094.

ZHOU, Y. 1993*b* Interacting scales and energy transfer in isotropic turbulence. *Phys. Fluids* A **5**, 2511–2524.

ZHOU, Y., YEUNG, P. K. & BRASSEUR, J. G. 1996 Scale disparity and spectral transfer in anisotropic numerical turbulence. *Phys. Rev.* E **53**, 1261–1264.